New insights into the Barremian–lower Aptian calcareous nannofossils of the Mediterranean Tethys: Chronostratigraphic and paleobiogeographic implications

Roque Aguado, Miguel Company, Luis O'Dogherty, José Sandoval, Mathieu Martinez

▶ **To cite this version:**

Roque Aguado, Miguel Company, Luis O'Dogherty, José Sandoval, Mathieu Martinez. New insights into the Barremian–lower Aptian calcareous nannofossils of the Mediterranean Tethys: Chronostratigraphic and paleobiogeographic implications. Marine Micropaleontology, 2022, 173, pp.102114. 10.1016/j.marmicro.2022.102114 . insu-03616872

HAL Id: insu-03616872
https://insu.hal.science/insu-03616872

Submitted on 23 Mar 2022

HAL is a multi-disciplinary open access archive for the deposit and dissemination of scientific research documents, whether they are published or not. The documents may come from teaching and research institutions in France or abroad, or from public or private research centers.

L'archive ouverte pluridisciplinaire **HAL**, est destinée au dépôt et à la diffusion de documents scientifiques de niveau recherche, publiés ou non, émanant des établissements d'enseignement et de recherche français ou étrangers, des laboratoires publics ou privés.

Distributed under a Creative Commons Attribution 4.0 International License

Journal Pre-proof

New insights into the Barremian–lower Aptian calcareous nannofossils of the Mediterranean Tethys: Chronostratigraphic and paleobiogeographic implications

Roque Aguado, Miguel Company, Luis O'Dogherty, José Sandoval, Mathieu Martinez

PII: S0377-8398(22)00030-5

DOI: https://doi.org/10.1016/j.marmicro.2022.102114

Reference: MARMIC 102114

To appear in: *Marine Micropaleontology*

Received date: 18 March 2021

Revised date: 19 January 2022

Accepted date: 16 March 2022

Please cite this article as: R. Aguado, M. Company, L. O'Dogherty, et al., New insights into the Barremian–lower Aptian calcareous nannofossils of the Mediterranean Tethys: Chronostratigraphic and paleobiogeographic implications, *Marine Micropaleontology* (2021), https://doi.org/10.1016/j.marmicro.2022.102114

This is a PDF file of an article that has undergone enhancements after acceptance, such as the addition of a cover page and metadata, and formatting for readability, but it is not yet the definitive version of record. This version will undergo additional copyediting, typesetting and review before it is published in its final form, but we are providing this version to give early visibility of the article. Please note that, during the production process, errors may be discovered which could affect the content, and all legal disclaimers that apply to the journal pertain.

© 2022 Published by Elsevier B.V.

Journal Pre-proof

New insights into the Barremian–lower Aptian calcareous nannofossils of the Mediterranean Tethys: chronostratigraphic and paleobiogeographic implications

Roque Aguado[a,*] raguado@ujaen.es, Miguel Company[b], Luis O'Dogherty[c], José Sandoval[b], Mathieu Martinez[d]

[a]Departamento de Geología and CEACTEMA, Universidad de Jaén, Campus Científico-Tecnológico de Linares, 23700 Linares, Spain

[b]Departamento de Estratigrafía y Paleontología, Universidad de Granada, 18002 Granada, Spain

[c]Departamento Ciencias de la Tierra, Universidad de Cádiz, CASEM, 11510 Puerto Real, Spain

[d]Univ Rennes, CNRS, Géosciences Rennes, UMR 6118, 35000 Rennes, France

[*]Corresponding author.

Journal Pre-proof

Abstract

A detailed study of calcareous nannofossil assemblages from twelve uppermost lower Barremian–lower Aptian sections in the Subbetic domain of the Betic Cordillera was performed. Seven new nannofossil species (*Crucibiscutum bastetanum*, *Crucibiscutum gracile*, *Chiastozygus improstauros*, *Cyclagelosphaera platyaspis*, *Lithraphidites aichmoides*, *Lithraphidites pugio*, and *Rhagodiscus sicutclipeus*) are described, one species is emended (*Lithraphidites magnus*) and the taxonomic concept of the marker species *Hayesites irregularis* is discussed and clarified. The detailed stratigraphic ranges of the new species, together with those of other relevant taxa, are determined and correlated to standard ammonite biostratigraphy. Age estimates of biostratigraphically relevant calcareous nannofossil biohorizons are calculated using astrochronologically tuned cyclostratigraphic data. Five new calcareous nannofossil subzones are proposed

which enhance upper Barremian biostratigraphic resolution at a regional scale and are directly correlated with respect to the standard Tethyan ammonite zonation. Two of the new species described here are used as biostratigraphic markers for the newly proposed subzones. The duration of each subzone is provided through astrochronological calibration. This study allows the refinement of the calcareous nannofossil zonation for the Mediterranean–Atlantic province of the Tethyan domain. The implications of these new results are discussed regarding the extant definition and use of the Barremian/Aptian boundary. The morpho-evolutionary trends of selected nannofossil groups are reviewed in relation to the latest Barremian–Aptian paleogeographic changes, showing these were a prominent factor controlling calcareous nannoplankton evolution and biogeographical distribution in the west European-Atlantic region.

Keywords: Taxonomy; Biometry; Biogeography; Bio-chronostratigraphy; Barremian–Aptian boundary; Betic Cordillera

1. Introduction

The Barremian Stage (~125.98 to ~121.40 Ma; Martinez et al., 2020) records a particular interval marked by notable environmental and biotic changes. These include two episodes of accelerated environmental change (e.g., Föllmi, 2012): the Mid-Barremian Event (MBE; Coccioni et al., 2003; Sprovieri et al., 2006; Yilmaz et al., 2012; Huck et al., 2013; Aguado et al., 2014a) and the Taxy Episode (TE; Masse and Machhour, 1998; Moullade et al., 1998a; Föllmi, 2012; Wissler et al., 2002; Godet et al., 2006; Stein et al., 2011; Martinez et al., 2020). Both episodes were linked to carbon-cycle perturbations locally related to enhanced preservation of organic-rich marine sediments.

One of the most convenient ways to identify these episodes is through their C-isotope imprints, as their lithological expression in different basins may vary depending on the local depositional and environmental conditions (e.g., Jenkyns, 2010). The calibration of the resulting C-isotope curves to biostratigraphy, chronostratigraphy, magnetostratigraphy and to geochronology will greatly impact global correlations (e.g., Ogg et al., 2016; Olierook et al., 2019; Gradstein et al., 2020; Martinez et al., 2020; Castro et al., 2021; Zhang et al, 2021).

Tethyan ammonite biostratigraphy (e.g., Reboulet et al., 2018) represents, in the Barremian, a high-precision reference scale to which C-isotope data could be tied. In the absence of ammonites, biostratigraphic scales based on calcareous nannofossils, planktonic foraminifera and/or radiolarians) may be used (e.g., Thierstein, 1971, 1973, 1976; Sissingh, 1977; Roth, 1978; Perch-Nielsen, 1985; Coccioni and Premoli-Silva, 1994; Jud, 1994; O'Dogherty, 1994; Bralower et al., 1995; Premoli-Silva et al., 2018). However, the biostratigraphic resolution of these microfossil groups is currently much lower compared to that obtained using ammonites. In addition, the calcareous nannofossil zonations have a low resolution with regard to counterpart schemes developed for the West European Province of the Boreal Realm (e.g., Jakubowski, 1987; Bown et al., 1998; Jeremiah, 2001). This may be due, in part, to the spread of sedimentary facies unfavorable for a good preservation of the taxa (i.e., limestones) in the Tethyan Realm, leading to a poor investigation in land sections where nannofossils can be correlated to other reference groups such as ammonites.

Journal Pre-proof

The Barremian successions of argillaceous limestones and marlstones of the Subbetic Domain in the Betic Cordillera are well dated by ammonites (e.g., Company et al., 1992, 1995, 2003; Aguado et al., 1992, 1997), and proved to contain abundant and moderately to well-preserved calcareous nannofossil assemblages (e.g., Aguado et al., 1997, 2014a). Some of these successions were also studied for C-isotope stratigraphy, both MBE and TE were identified in them (e.g., Aguado et al., 2014a; Martinez et al., 2020), and they have been recently calibrated by astrochronology (Martinez et al., 2020). These successions represent good candidates to improve Tethyan calcareous nannofossil biostratigraphy by providing adequate chronostratigraphical and geochronological frameworks to tie all the biostratigraphic events.

The aim of this paper is to improve the resolution of the Barremian calcareous nannofossil biozonation for the Mediterranean so it can be used as an alternative to ammonite zones. The stratigraphic range of the calcareous nannofossil species with biostratigraphic potential, together with that of other relevant taxa, will be directly correlated to standard ammonite biostratigraphy and to the geochronologic scale. Finally, as the Barremian/Aptian boundary is included within the interval studied, it will be discussed in the light of new findings.

2. Geological setting

All sections studied belong to the Subbetic Domain (Fig. 1), a complex tectonostratigraphic unit that paleogeographically corresponds to the pelagic areas of the southern passive margin of the Iberian Plate during the Alpine tectonic cycle (Triassic to early Miocene). During the Jurassic and Early Cretaceous this region underwent extensional tectonics associated with the seafloor spreading of the North Atlantic in a

transform continental margin setting (Vera, 2001, 2004; Martín-Chivelet et al., 2019). A paleolatitude of ~26–28º N (Fig. 2) has been inferred for the Barremian–early Aptian position of the Subbetic Domain (e.g., Barron et al., 1981; Stampfli and Kozur, 2006; Cao et al., 2017; Barrier et al., 2018), being located near the boundary between the arid-tropical and humid-temperate climatic belts (e.g., Masse et al., 1993; http://www.scotese.com/ecretcli.htm; Fig. 2).

Except for $X.Cp_2$ section (see Chapter 3), all sections studied belong to the widely extended Lower Cretaceous Carretero Formation (Figs. 3, 4). Roughly, the lithologic succession of this formation (e.g., de Gea, 2004) consists of a rhythmic alternation of yellowish to gray argillaceous limestone beds (5–90 cm thick) and gray marlstone interbeds (3–760 cm thick). The lime fraction is partially made up of calcareous nannofossil remains and carbonate particles of micritic size (micarbs) which probably originated from the adjacent platforms. Clay minerals are, by far, the main components of the detrital fraction (e.g., Aguado et al. 2008). Overlying the Carretero Formation, some sections include parts of the Argos, Fardes, or Carbonero formations (Figs. 3, 4; see also Supplementary Material 1 (SM1) for details on lithostratigraphy and biostratigraphy).

Journal Pre-proof

3. Material and methods

A total of 575 samples, spread across 12 sections were studied. These include, from West to East (Fig. 1):

- Caprés (A in Fig. 1. Section $X.Cp_2$; 38.233078°N, 1.134206°W; 16 samples; Fig. 4).
- Arroyo de Gilico (B in Fig. 1. Section $X.V_1$; 38.159931°N, 1.678208°W; 77 samples; Fig. 3).

- Barranco de Cavila (C in Fig. 1. Section X.Kv: 38.051514°N, 1.885713°W; 57 samples; Fig. 3. Section X.Kv_2: 38.052469°N, 1.888964°W; 222 samples; Fig. 3).

- Río Argos (D in Fig. 1. Section X.Ag6: 38.051514°N, 1.885713°W; 15 samples; Fig. 4).

- Rambla Seca (E in Fig. 1. Section RA03: 37.794622°N, 2.030255°W; 32 samples; Fig. 3).

- Cerro Trompeta y Cortijo del Hielo (F in Fig. 1. Section X.CT: 37.866290°N, 2.575907°W; 8 samples; Fig. 4. Section X.HA: 37.851783°N, 2.588921°W; 29 samples; Fig. 4).

- Barranco de las Azadillas (G in Fig. 1. Section X.Z: 37.779300°N, 2.708924°W; 12 samples; Fig. 4).

- La Frontera (H in Fig. 1. Section X.F: 37.591233°N, 3.602561°W; 56 samples; Fig. 4. Section X.F1: 37.593226°N, 3.603832°W, 39 samples; Fig. 4).

- La Coronilla (I in Fig. 1. Section X.CO_2: 37.546093°N, 3.937009°W; 13 samples; Fig. 4).

Although sections X.Cp_2, RA03, X.CT, X.HA, X.F, X.F1 and X.CO_2 have been studied previously (see SM1), new smear-slides were prepared and studied for all samples. Samples from X.V_1, X.Kv, X.Kv_2, X.Ag6 and X.Z sections (370) are new. The number of samples studied in each section and their respective positions are stated in figures 3, 4, and in Supplementary Material 2 (SM2). The sampling intervals were highly variable (Figs. 3 and 4), from 6–7 cm (e.g., sections X.V_1 and X.Kv_2) to several meters (e.g., lower part of X.F section). Except for samples from the RA03 section and those from the uppermost Barremian to lower Aptian parts of the X.F and X.F1 sections, the remainder of them are directly correlated to ammonite zones/subzones (Aguado, 1994;

Aguado et al., 1992, 1997, 2017; Company et al., 1995, and this paper). In the present work, the standard ammonite zonation for the Mediterranean Province (Reboulet et al., 2018) is followed, and used as a reference to calibrate the calcareous nannofossil bioevents. In the absence of magnetostratigraphical data, the base of the *Deshayesites oglanlensis* ammonite Zone (AZ) is used here to determine the base of the Aptian (Reboulet et al., 2011, 2018).

Simple permanent smear slides (Bown and Young, 1998) were mounted with coverslips for routine biostratigraphic analysis and examined for nannofossil content using a polarizing light microscope Olympus BHSP at 1200 × magnification. At least a complete longitudinal traverse (= 200 fields of view; surface area of one field = 2.37 × 10^{-2} mm^2) was studied, but in some slides several (up to 4) longitudinal traverses were studied. Special care was taken to prepare the smear slides as uniformly as possible, so that particle density on the slide surface was kept between 30–50% (Baccelle and Bosellini, 1965). To determine the stratigraphic position of the horizon from which the wide-canal nannoconids are more abundant than narrow-canal nannoconids (wc>nc Event) in some sections (RA03, X.F, X.HA, X.Kv and X.Kv_2), nannoconids were counted in 50 fields of view on samples selected according to their biostratigraphic position. The percentages of wide canal (including *Nannoconus bucheri*, *N. circularis*, *N. truittii*; *N.* sp. cf. *N. truittii*, *N. vocontiensis* and *N. wassallii*) and narrow canal (including *Nannoconus bermudezii* and *N. steinmannii*) forms were calculated (see SM2). The used taxonomic framework is based on Perch-Nielsen (1985), Bown (1998, 2005), Aguado et al. (1997, 2014b, c), and the nannotax website (http://www.mikrotax.org/Nannotax3/index.php?dir=Mesozoic).

Journal Pre-proof

Preservation in the assemblages was evaluated in each sample (see SM2) based on the visual criteria established by Roth and Thierstein (1972) and Roth (1983). Limestone beds were avoided for sampling, as they contain impoverished (poorly to moderately preserved) assemblages with moderate to heavily overgrown taxa. Overall abundance per sample was estimated by counting the total number of nannofossils in 20 random fields of view.

Photomicrographs of calcareous nannofossils were acquired with an Olympus Camedia C5050 camera attached to the Olympus BHSP microscope, using cross-polarized light (XPL). A wide variability of size was observed for some taxa recorded throughout the studied interval. To test whether size of specific taxa fluctuates throughout the studied interval, specimens of *Lithraphidites* spp. (120), *Hayesites irregularis* group (140) and *Flabellites oblongus* (120) were photographed and measured. In addition, some specimens (6–22) of the new species described were also photographed and measured. The results are documented in the SM2. Measurements were taken using ImageJ software, with an accuracy of ± 0.03 μm. Regarding precision, in a set of 10 repetitive measurements of 10 specimens, the error was lower than ±0.14 μm with a 95% confidence level. The lengths (L) and widths (W) of *Lithraphidites* spp., *H. irregularis* gr. and *F. oblongus* specimens were later used to test whether these three groups consist of several taxa.

To test the supposed multimodality in the populations of the measured taxa, mixture analyses were applied to the whole data sets, (i.e., all specimens of each group pooled together) using the free PAST v4.05 software package (Hammer et al., 2001). This statistical analysis is a maximum-likelihood method for estimating the descriptive

parameters (mean, standard deviation and proportion) of two or more distinct distributions, based on an initially pooled univariate sample (Hammer and Harper, 2006). The minimum values of the Akaike Information Criterion (AIC, Akaike, 1974) helped to identify the groups obtained by mixture analysis with the lowest overfitting (Hammer et al., 2001). The number of bins for histograms in mixture analyses follows the Sturges' rule ($k = (\log_2 n) + 1$), where k is the number of bins and n the number of observations).

4. Results

4.1 Nannofossil abundance and preservation

Calcareous nannofossil abundance usually fluctuates between > 5 and 30 specimens per field of view (SFOV), with only discrete samples showing abundances below 5 SFOV, while 22 samples were barren (see SM2). Nannofossil assemblages are rich and moderately to well preserved, showing slight to moderate overgrowth except for those from the organic-rich beds of X.Ag3 and X.Z sections, which showed moderate to strong etching (see SM2).

4.2 Mixture analyses

Fluctuations observed in length (L) and width (W) in the pool of the measured specimens of *Lithraphidites* spp. (Fig. 5A–D) suggest that several species can be differentiated. The results of a mixture analysis performed on the W values (Fig. 5E) reveal three different-sized groups. The first group corresponds to *L. carniolensis* (Fig. 5A), while the second and third group correspond to *L. aichmoides* (Fig. 5B; Chapter 6) and to the *L. pugio*/*L. magnus* plexus respectively (Fig. 5C, D). The same statistical analysis was applied to the length (L) of all specimens with W greater than 4.5 μm (*L.*

pugio/*L. magnus* plexus). The frequency histogram (Fig. 5G) reveals the existence of two different-sized groups, which represent the new species *L. pugio* and *L. magnus* (Fig. 5C, D; Chapter 6). Figure 5H shows the descriptive parameters resulting from the mixture analysis performed on W in the whole data set and on L in those specimens having a W greater than 5 μm. However, total length (L) proved not to be an outright criterion to separate the latter two species, being more effective distinguishing both taxa using the L/W ratio (Fig. 6; see also Chapter 6).

Hayesites irregularis is an important marker species in the Tethyan Realm (e.g., Thierstein, 1973; Perch-Nielsen, 1985; Bralower et al., 1995). Its taxonomic clarification can increase the biostratigraphic precision of stratigraphic correlations. Variations observed in the length (L) and width (W) of the specimens measured in this study (Fig. 7A, B) suggest the presence of two morphotypes in the *H. irregularis* group (gr.). This was corroborated by the results of a mixture analysis on the L/W ratio of the complete pool of measurements (Fig. 7C). Forms with a nearly circular outline, (L/W smaller or equal to 1.12), being younger in time, were assigned to *H. irregularis* sensu stricto (s.str.). Specimens having a more elongated outline (L/W>1.12) and poorly defined elements, being slightly older, were assigned to *H. irregularis* morphotype E (*H. irregularis* E; Chapter 6).

Mixture analyses performed on size measurements (L and W) of specimens of *Flabellites oblongus* sensu lato (s.l.) spread across the uppermost lower Barremian–lower Aptian of the study sections (see SM2 and Fig. 8) provided non-conclusive results. These showed similar AIC values for unimodal/bimodal solutions suggesting a

rather continuous increase in size through the complete data pool (Fig. 8) thereby hindering a clear separation of different populations (see Chapter 6).

4.3. Sequence of nannofossil bioevents

One hundred and four taxa were identified through the complete interval studied, including 7 new species (see SM2 and Chapter 6). The following sequence of bioevents (from bottom to top) has been observed:

- Presence of *Braarudosphaera hockwoldensis* (*Holcodiscus fallax* ammonite subzone [ASz]).
- Lowest occurrence (LO) of *Flabellites oblongus* (*Holcodiscus caillaudianus* ASz).
- LO of *Lithraphidites aichmoides* (*Moutoniceras moutonianum* ammonite zone [AZ]).
- Successive LOs of *Phosterolithus prossi*, *Crucibiscutum gracile* and *Lithraphidites pugio* (*Gassendiceras alpinum* ASz).
- LO of *Rhagodiscus sicutclipeus* (uppermost part of the *Gerhardtia sartousiana* ASz).
- Successive LOs of *Chiastozygus lamprostauros*, *Micrantholithus stellatus* and *Rhagodiscus gallagheri* (*Gerhardtia provincialis* ASz).
- LO of *Hayesites irregularis* E, highest occurrences (HOs) of *Lithraphidites pugio* and *Lithraphidites aichmoides*, followed by the successive LOs of *Lithraphidites magnus*, *Crucibiscutum bastetanum* and *Nannoconus* sp. cf. *N. truittii* (*Hemihoplites feraudianus* ASz).
- LO of *Hayesites irregularis* s. str. (*Imerites giraudi* AZ)
- LO of *Stoverius acutus*, followed by the wc>nc Event and the HO of *Crucibiscutum bastetanum* (lower part of the *Martelites sarasini* AZ).
- LOs of *Nannoconus truittii* and *Rhagodiscus angustus* (*Deshayesites oglanlensis* AZ).

Journal Pre-proof

- Presence of *Conusphaera rothii* and *Micrantholithus stellatus* (lower part of the *Deshayesites forbesi* AZ).

A summary of the main bioevents recorded and their stratigraphic context is shown in Figure 9.

5. Discussion

5.1. Biostratigraphic remarks

Although most of the taxa shown in Figure 9 have stratigraphic value, several of them (e.g., *Chiastozygus lamprostauros*, *Crucibiscutum gracile*, *Lithraphidites magnus*, *Nannoconus* sp. cf. *N. truittii*, *Phosterolithus prosii*, *Rhagodiscus sicutclipeus* and *Stoverius acutus*) are rare and/or have a spotty and discontinuous record (drawn in dashed line in Fig. 9) throughout a substantial part of their respective stratigraphic ranges.

Other taxa have unclear LOs due to the presence of transitional morphologies in the stratigraphic record. Such is the case of the LOs of *Rhagodiscus gallagheri* (obscured by the presence of transitional forms from small *Rhagodiscus asper*) and *Lithraphidites magnus* (difficult to differentiate from transitional specimens from *Lithraphidites pugio* in the upper part of the *Hemihoplites feraudianus* ASz). The LO of *Nannoconus truittii* (upper part of *Deshayesites oglanlensis* AZ) is masked by the record of forms similar to this species reported here as *Nannoconus* sp. cf. *N. truittii* (see Chapter 6: Figures 3, 4, and range charts of SM2). Finally, specimens of *Rhagodiscus gallagheri* transitional to *Rhagodiscus angustus* were observed from the upper part of the *Martelites sarasini* AZ. The oldest forms assignable to *R. angustus* were recorded from the uppermost part of

the *Deshayesites oglanlensis*/lowermost *Deshayesites forbesi* AZs upwards, which agrees with the observations of Rutledge and Bown (1996).

Other bioevents, such as the FOs of *Flabellites oblongus* and *Hayesites irregularis* have been used as biostratigraphic markers (e.g., Thierstein, 1973, 1976; Bralower et al.1995), but they were never adequately correlated to ammonite biostratigraphy. The LO of *F. oblongus* was recently identified in the lower part of the *Moutoniceras moutonianum* AZ (Aguado et al., 2014a; Martinez et al., 2020). Here we report the LO of *F. oblongus* from the *Holcodiscus caillaudianus* ASz in the X.Kv and X.V_1 sections. This species is very rare and shows a spotty record throughout the *H. caillaudianus* ASz and lowermost part of the *M. moutonianum* AZ. Its consistent record (Figs. 3, 9) correlates with the level where Aguado et al. (2014a) and Martinez et al. (2020) reported the LO of this species. *Hayesites irregularis* E is rather rare near its LO and is more abundant from the upper part of the *Hemihoplites feraudianus* ASz. The LO of *H. irregularis* s.str. (Chapter 4.3 and Fig. 9) was not recorded until the mid part of the *Imerites giraudi* AZ (Figs. 3, 4; SM2).

Finally, a small group of taxa have shown fairly continuous and consistent records. These include *Lithraphidites pugio*, whose LO was already successfully used in regional correlation (as *L.* sp. cf. *L. magnus*) by Martinez et al. (2020), *Micrantholithus stellatus*, and the distinctive *Crucibiscutum bastetanum* (Fig. 9 and SM2). In addition, the stratigraphic horizon from which the proportion of wide-canal nannoconids outnumber the narrow-canal nannoconids (wc>nc Event, Figs. 3, 4, 9; sections X.HA, X.Kv, X.Kv_2 and SM2), has also proven to be a good correlation event. In some sections (RA03, X.F, X.F1), this horizon is masked by a stratigraphic break surface (see

Figs. 3, 4, and SM2). The onset of the 'nannoconid decline' event (e.g., Erba et al., 1999, 2019; Channell et al., 2000; Erba 2004; Tremolada et al., 2006) was not determined in this study.

5.2. Proposed biozones

Here we document a detailed zonation of the upper Barremian–lower Aptian interval of the Mediterranean area. The zonation uses the scheme of Bralower et al. (1995) by adding new subzones as digits. The proposed subzones are useful on a regional scale (e.g., Martinez et al., 2020), but they could be applied to the Mediterranean–Atlantic area, as some of the marker species were also recorded from outside of the Betic Cordillera (chapters 5.4, 6).

NC5E1 Subzone. (New subzone)

Base: LO of *Flabellites oblongus*. Calibrated here to 124.72 Ma, slightly earlier than in Martinez et al. (2020). This bioevent also corresponds to the base of the NC5E Subzone (Bralower et al., 1995).

Top: LO of *Lithraphidites pugio* (calibrated to 123.57 Ma).

Age and stratigraphic range: Latest early Barremian–earliest late Barremian (upper part of the *Holcodiscus caillaudianus* ASz–lower part of the *Gassendiceras alpinum* ASz). This subzone has a duration of 1.15 myr following the chronostratigraphy of Martinez et al. (2020).

NC5E2 Subzone. (New subzone)

Base: LO of *L. pugio*.

Top: LO of *Micrantholithus stellatus* (calibrated to 122.64 Ma).

Journal Pre-proof

Age and stratigraphic range: Mid-part of the late Barremian (lower part of the *G. alpinum* ASz–upper part of the *Gerhardtia provincialis* ASz). Duration of 0.93 myr according to Martinez et al. (2020).

NC5E3 Subzone. (New subzone)

Base: LO of *M. stellatus*.

Top: LO of *Hayesites irregularis* E (calibrated here to 122.45 Ma), slightly earlier than in Martinez et al., (2020).

Age and stratigraphic range: Mid-part of the late Barremian (upper part of the *G. provincialis* ASz–lower part of the *Hemihoplites feraudianus* ASz). Duration of 0.19 myr following Martinez et al. (2020).

NC6A1 Subzone. (New subzone)

Base: LO of *H. irregularis* E.

Top: HO of *Crucibiscutum bastetanum* (calibrated here to 121.97 Ma).

Age and stratigraphic range: Upper part of the late Barremian (lower part of *H. feraudianus* ASz–lower part of *Martelites sarasini* AZ). Duration of 0.48 myr following Martinez et al. (2020).

NC6A2 Subzone. (New subzone)

Base: HO of *C. bastetanum*.

Top: HO of *Conusphaera rothii*.

Age and stratigraphic range: Latest Barremian–early Aptian (lower part of the *M. sarasini* AZ–*Hedbergella excelsa*). This subzone has a duration much greater than 0.97 myr following Martinez et al. (2020).

Journal Pre-proof

5.3. Calcareous nannofossil bioevents, C-isotope stratigraphy and the Barremian/Aptian boundary: an update

Currently, the boundary between the Barremian and Aptian Stages is provisionally located at the base of the CM0r magnetochron, and the Gorgo a Cerbara section is its possible Global Stratotype Section and Point (Erba et al., 1996). This designation was made based on the supposed proximity of the lower boundary of CM0r to the LO of deshayesitid ammonites (=base of the Aptian used by ammonite specialists; e.g., Reboulet et al., 2018). However, magnetostratigraphic record is very poorly preserved in hemipelagic sections where ammonite zonations are established and, to date, no direct calibration of magnetic polarity and ammonite zones is so far available for the upper Barremian–lowermost Aptian interval.

The LO of *Hayesites irregularis* has been reported in Gorgo a Cerbara from ~6 m below the base of CM0r (Patruno et al., 2015). New findings (Martinez et al., 2020, and present paper) indicate that the LO of *H. irregularis* gr. occurs in the lower part of the *Hemihoplites feraudianus* AS z (see chapters 4.3 and 5.1), below that reported by Aguado et al. (1997). This is consistent with the stratigraphy of Gorgo a Cerbara proposed by Frau et al. (2018), and indicates that the LO of *H. irregularis* is far below the base of the Aptian as defined by the first appearance of deshayesitids.

The wc>nc Event (e.g., Erba et al., 1999; Larson and Erba, 1999; Channell et al., 2000; Bellanca et al., 2002; Tremolada et al., 2006; Erba et al., 2019) was recorded in the Gorgo a Cerbara section within CM0r (Channell et al., 2000; Patruno et al., 2015). This horizon has been here correlated to the lower part of the *Martelites sarasini* AZ (Figs. 3,

4, 9 and SM2). This change in the proportions of narrow/wide canal nannoconids requires time-consuming analyses to be determined, and probably is not a good alternative as a primary marker to be used in the definition of the base of the Aptian, but it could be used as a secondary indicator at least in the Tethyan Realm.

The HO of the new coccolith species *Crucibiscutum bastetanum* follows the wc>nc Event and slightly predates the onset of the C-isotope Intra-Sarasini Negative Excursion (ISNE) linked to the Taxy Episode (Föllmi, 2012; Frau, 2020; Martinez et al., 2020). According to the chronology of Martinez et al. (2020), this bioevent predates the Barremian/Aptian boundary by 0.57 myr, being a moderately good approximation to it. However, this new species has been identified only in the Subbetic Domain as yet.

The LOs of *Nannoconus truittii* and *Rhagodiscus angustus* (upper part of *Deshayesites oglanlensis*–lower part of *Deshayesites forbesi* AZs) do not provide reliable events because they are masked by the presence of specimens with transitional morphologies (see chapters 5.1 and 6). No other reliable calcareous nannofossil event has been recorded from the Betic Cordillera, until the 'nannoconid crisis', which has been correlated to the upper part of the *D. forbesi* AZ (Aguado et al., 1999; Moreno-Bedmar et al., 2009, 2012).

The C-isotope ISNE, has been identified in several sections within the mid–upper part of the *Martelites sarasini* AZ (Kuhnt et al., 1998; Moullade et al., 1998a, b; Godet et al., 2006; Frau, 2020; Martinez et al., 2020). Its top is close to the base of the Aptian as defined by ammonite biostratigraphy. In sections from SE France and Spain (see also Sanchez-Hernandez and Maurrasse, 2016), the ISNE is made of two spikes with lower

C-isotope values separated by a short excursion with slightly higher values (Fig. 10). In the Gorgo a Cerbara section the ISNE consists of only one spike in the $\delta^{13}C$ curve, which is located at the top of CM0r and correlates with the change from the 'Maiolica' to the 'Marne a Fucoidi' formations (e.g., Godet et al., 2006; Stein et al., 2011; Frau et al., 2018).

Figure 10 summarizes the findings of the current study around the Barremian–Aptian interval and correlates the $X.Kv_2$ section and some relevant French and Italian sections by using bio- and chemostratigraphy. Given the proximity of the ISNE (especially its top) to the base of *D. oglanlensis* AZ, we think this negative excursion of the $\delta^{13}C_{carb}$ is an alternative for defining the base of the Aptian.

5.4. Barremian–Aptian calcareous nannofossil morpho-evolutionary trends and paleobiogeography

Although the driving factors for size changes of calcareous nannofossils have been discussed in the last decades, both for living assemblages and for fossil species, these remain still unclear. In living assemblages, some link was found within coccolith morphology and environmental factors such as sea-water temperature and salinity (e.g., Bollmann and Klaas, 2008; Bollmann et al., 2009; Triantaphyllou et al., 2010). In deeper time, studies are more problematic due to difficulties in the reconstruction of the paleoenvironmental conditions and the effects of preservation in the fossil assemblages. Despite this, factors such as sea-water temperature (e.g., Bornemann and Mutterlose, 2006; Linnert and Mutterlose, 2013; Wulff et al., 2020), nutrient (e.g., Erba et al., 1995; Giraud et al., 2006; Linnert and Mutterlose, 2013; Lübke et al., 2015; Wulff et al., 2020) and light availability (e.g., Lübke et al., 2015; Lübke and Mutterlose, 2016),

acidification (e.g., Erba et al., 2010), or trace metal- and CO_2 water concentrations (e.g., Faucher et al., 2017) are thought to have influenced coccolith growth and calcification. Coccolith size change in the fossil record has been also attributed to evolutionary processes (López-Otálvaro et al., 2012; Gollain et al., 2019). Changes toward decreasing size are usually claimed to represent a response to stressful and unstable environmental conditions (eutrophication, lower temperature and light availability, increased CO_2 concentrations and acidification) in some fossil coccolith species, while other taxa do not show size alterations. Long-term size increases are however claimed to be related to evolutionary processes. Since most of the observed biometric changes in this study (e.g., in *Flabellites oblongus*, in the new *Lithraphidites* morphospecies and in the *Hayesites irregularis* gr.) represent mainly long-term size increases, they are interpreted as related to evolutionary processes.

The biometric studies cited above were all performed on coccolith species. However, most of the biometric data presented in this study correspond to nannoliths whose possible relationship with coccoliths is uncertain and whose ecological preferences are mostly unknown.

However, our data suggest that some link existed between morphologic change/evolutionary patterns and paleogeography. Here we review the morpho-evolutionary trends of selected nannofossil groups in relation to the latest Barremian–Aptian paleogeographic changes.

The genus *Lithraphidites* first appeared in the Berriasian (e.g., Perch-Nielsen, 1985) and consist of bladed rod-shaped nannoliths that taper towards both ends, have a cruciform

cross-section and may have a minute basal murolith coccolith. Janin (1988) suggested affinities of these nannoliths with Actinozoa that most authors do not find compelling, and it is currently thought that they may represent disarticulated spines of a heterococcolith (https://www.mikrotax.org/system/index.php?taxon=Lithraphidites&module=ntax_mesozoic).

A common evolutionary trend within the genus *Lithraphidites* consists of a widening of the longitudinal blades in a symmetrical or asymmetrical way. This trend episodically originated in several species across the Cretaceous (e.g., *L. houghtonii* and *L. moray-firthensis* in the Aptian; *L. alatus*, *L. acutus* and *L. eccentricus* in the Albian-Cenomanian; *L. praequadratus*, *L. quadratus* and *L. kennethii* in the Campanian-Maastrichtian). The current work shows this trend also operated on the Tethyan–Atlantic *Lithraphidites* across the latest early Barremian–late Barremian (Figs. 11, 12, 13), leading to the differentiation of three species (*L. aichmoides*, *L. pugio* and *L. magnus*; Chapter 6). These constitute the earlier known record of this evolutionary trend within the genus *Lithraphidites*.

Besides the Subbetic Domain, *L. magnus* was recorded in the North American Basin (Covington and Wise, 1987), West Iberian Continental Margin (Bralower et al., 1994) and northern Gargano (Cobianchi et al., 1997). This suggests a westernmost Tethys–North Atlantic paleogeographic record for this species (Fig. 2). The records of *L. aichmoides* and *L. pugio* are so far limited to the Subbetic as both are new species described in the current work and remain undifferentiated from *L. magnus* in the previous papers.

Journal Pre-proof

Lithraphidites houghtonii is a species with a very similar morphology to *L. pugio*/*L. magnus*, but being noticeably smaller (length 9–12 µm). It was recorded (Jeremiah, 2001; Bottini and Mutterlose, 2012) throughout the lower Aptian (uppermost part of *Prodeshayesites fissicostatus* AZ) to lower upper Aptian of the North Sea area and Lower Saxony Basin (Fig. 2). As the evolutionary lineage defined by the Tethyan–Atlantic *L. aichmoides-L. pugio-L. magnus* is earlier, we speculate these taxa (especially *L. magnus*) could be the ancestors of the Boreal species. In relation to this, the latest Barremian–early Aptian paleogeography (Fig. 2), together with sea level rise (e.g., Hallam, 1992; Mutterlose, 1992b; 1996; Hardenbol et al., 1998; Mutterlose and Böckel, 1998) would have allowed the migration of some populations of *L. magnus* into the North Sea Basin, where they evolved into *L. houghtonii* (Fig. 11). Several authors record a homogenization followed by a Tethyan influx of marine invertebrate faunas (Mutterlose, 1987, 1998; Mutterlose and Böckel, 1998) and calcareous nannofloras (Mutterlose, 1987, 1989, 1992a, 1996; Jeremiah, 2001) into the West European Province (WEP) of the Boreal Realm throughout the early Aptian, which gives additional support to the suggested migration.

The marker species *Flabellites oblongus* and *Hayesites irregularis* gr. also underwent morphologic changes across the late Barremian–early Aptian here interpreted as the result of long-term evolutionary processes. The early coccoliths of *F. oblongus* are small, progressively increasing to medium size from the *Gerhardtia provincialis* ASz upwards (Figs. 8, 9; see Aguado et al., 1997; Bown, 2005). Regarding the *H. irregularis* gr., aside from the two morphotypes identified by mixture analyses (Chapter 4.2, 6; Fig. 7), a gradual increase in size has been observed in the specimens of *H. irregularis* s.str.

across the *Martelites sarasini* AZ (SM2). The LOs of *F. oblongus* and *H. irregularis* are often recorded, as rare species, from the lower Aptian interval (*Prodeshayesites fissicostatus*/*tenuicostatus–Deshayesites forbesi* AZs) in the WEP of the Boreal Realm (e.g., Erba et al., 1996; Bown et al., 1998; Mutterlose and Böckel, 1998; Jeremiah, 2001). However, these records correspond to the entry of the species in the Boreal Realm, which is concomitant with the homogenization of floras and faunas and Tethyan influx described above, and do not correspond to the true LOs of these species.

During the late Barremian, the WEP of the Boreal Realm and the Tethyan Realm were nearly isolated from each other (e.g., Ziegler, 1990; Mutterlose, 1992b; Barrier et al., 2018). However, Jeremiah (2001) recorded short influxes of *Micrantholithus stellatus* in rocks equivalent to the uppermost Barremian *Parancyloceras bidentatum* AZ in the North Sea Basin (Fig. 2). The LO of *M. stellatus* in the Subbetic Domain has been recorded in the upper part of the *Crioceratites gardtia provincialis* ASz (see chapters 4.3 and 5.1, Fig. 9), that is, much earlier than its occurrence in the North Sea Basin. Based on its morphological similarities with the extant species *Braarudosphaera bigelowii*, the genus *Micrantholithus* is commonly interpreted as a marginal/neritic taxon (e.g., Roth, 1994; Applegate et al., 1989; Street and Bown, 2000; Bown, 2005; Bottini and Mutterlose, 2012; Quijano et al., 2012; Aguado et al., 2014a, b). The short influxes of *M. stellatus* in the North Sea Basin suggest that shallow seaways intermittently connected the WEP of the Boreal Realm and the Tethyan Realm already during the late Barremian, favoring the expansion of Tethyan neritic nannofloras into the Boreal Realm. As no Boreal taxa were recorded in our sections during this interval, we suggest this influx of neritic Tethyan taxa (*M. stellatus*) into the Boreal Realm was probably favored by increasing temperatures related to the Taxy Episode.

Late Barremian episodes of sea isolation, coincident with regressive periods, favored the allopatric speciation of calcareous nannoplankton and the apparition of endemic taxa under restricted conditions, (e.g., in the WEP of the Boreal Realm; Jakubowski, 1987; Crux, 1989; Bown et al., 1998; Jeremiah, 2001). During moderate to extensive high stands, seaways opened improving the communication between the Tethyan Realm and the WEP of the Boreal Realm, and nannofloral exchange (e.g., Mutterlose, 1992a, b, 1996). All the described biogeographic data suggest that paleogeography played a fundamental role in the evolution and spatial distribution of calcareous nannoplankton in the west European-Atlantic region during the late Barremian–early Aptian interval.

6. Systematic paleontology (by R. Aguado)

The taxonomic descriptions below follow the terminology guidelines of Young et al. (1997) and the higher taxonomy follows Bown and Young (1997). Only taxonomic references that do not appear in Bown (1998) or cannot be found in the Nannotax website (http://www.mikrotax.org/Nannotax3/) are provided in the reference list. In the following descriptions, L = length, W = width, XPL = cross-polarized light, CNZ /CNSz = calcareous nannofossil Zone/Subzone.

Images and smear slides of type material are stored in the Department of Geology of the University of Jaén (DG image numbers bracketed in the descriptions below). All species names are registered at the Plant Fossil Names Registry (PFNR; https://plantfossilnames.org) of the National Museum Prague. The corresponding PFNR nomenclatural act number is indicated for each new species. The reference calcareous nannofossil biozonation used is that of Bralower et al. (1995), with the modifications

introduced in this paper. The reference planktonic foraminifera biozonation is that of Coccioni et al. (2007).

Order Podorhabdales Rood et al., 1971, emend. Bown, 1987

Family Biscutaceae Black, 1971

Genus *Crucibiscutum* Jakubowski, 1986

Crucibiscutum bastetanum sp. nov.

PFNR: PFN001007.

(Figs. 14A–N)

1997 *Crucibiscutum salebrosum* Aguado et al., Figs. 8.19, 8.20, 8.22 *non* Fig. 8.21.

2014a *Crucibiscutum hayi* Aguado et al., Figs. 4.8–4.10.

2014b *Crucibiscutum hayi* Aguado et al., Fig. 8.15.

Derivation of name: After the *Bastetani*, an old Iberian tribe that populated the southeastern part of the Iberian Peninsula, the type area of this species.

Diagnosis: Small to medium sized (3.4–5.5 μm) broadly elliptical to normally elliptical *Crucibiscutum* coccoliths with a relatively narrow central area spanned by off-axial (slightly rotated) cross bars. The rim is bicyclic, with the bright inner cycle being wider (~1 μm width) than the outer dark cycle.

Description: Under XPL, the bright inner cycle of the rim has equal or greater width than the outer dark cycle. The central area is nearly filled by a relatively thick cross slightly rotated with respect to the axes of the ellipse defined by the rim. The cross is bright (although not as bright as the inner cycle of the rim) under XPL when oriented at 45°, and dark when oriented to 0°. The long and short arms of the central cross usually have slightly different rotation.

Dimensions: L = 3.4–5.5 (average 4.6) μm; W = 2.9–4.5 (average 3.8) μm; specimens measured: 22.

Holotype: Figs. 14A, B [DG2802, DG2803] (are same specimen). Holotype dimensions: L = 4.9 μm, W =3.9 μm.

Paratypes: Figs. 14C, D [DG2804, DG2805] (are same specimen); Figs. 14E, F [DG2806, DG2807] (are same specimen).

Type level: Uppermost Barremian, sample X.HA-2 [DGF001] (NC6A1) nannofossil Subzone; upper part of *Imerites giraudi* AZ).

Type locality: X.HA section, Province of Granada, southeastern Spain.

Occurrence: This species has a short range. Its LO was found near the top of the *Gerhardtia sartousiana* AZ, (upper part of the *Heminoplites feraudianus* ASz), which is equivalent to the lowermost part of the NC6A1 CNSz, and is shortly preceded by the LO of the primitive forms (elongated) of *Hayesites irregularis* E. Its HO was recorded in the lower part of the *Martelites sarasini* AZ (upper boundary of the NC6A1 CNSz), shortly following the nc>wc Event (Chapter 4.3, Fig. 9). Usually this species is a rare component of the assemblages, being more abundant from the upper part of the *Imerites giraudi* AZ to its HO, but shows a rather consistent record. It was recorded in sections $X.Ag_6$, X.F, X.F1, X.HA, X.Kv, $X.Kv_2$, and RA03 from the Subbetic Domain in the Betic Cordillera (southern Spain). Its HO is used here to define the upper boundary of the NC6A1 CNSz.

Remarks: *Crucibiscutum bastetanum* differs from *Crucibiscutum salebrosum* (Berriasian–Hauterivian), *Crucibiscutum ryazanicum* (Berriasian–Valanginian) and *Crucibiscutum pinnatus* (Hauterivian–Barremian) by having a rim with a wider (~1 μm) bright inner cycle when viewed in XPL and a slightly larger size. *Crucibiscutum salebrosum* has, in addition, a cross aligned with the axes of the ellipse instead of a

slightly rotated one as in *C. bastetanum*. *Crucibiscutum bastetanum* differs from *Crucibiscutum neuquenensis* (lower Hauterivian) and *Crucibiscutum trilensis* (upper Hauterivian) by having a narrower central area, which is nearly filled by a relatively thick cross, and a wider (~1 μm) bright cycle of the rim when viewed in XPL. *Crucibiscutum hayi* (Upper Albian) and *Crucibiscutum gracile* (below) have wider (more open) central areas and narrower axial cross bars. *Palaeopontosphaera giraudii* (de Kaenel, 2020) has a greater size, with a bright inner cycle of the rim of similar width to the outer dark cycle, and an axial cross. Following de Kaenel et al. (2020), the range of *P. giraudii* is early Hauterivian–late Barremian (HO in *P. vandenheckii* AZ), being earlier in time than *C. bastetanum* and there is a stratigraphical displacement between these two species.

Crucibiscutum gracile sp. nov.

PFNR: PFN001008.

(Figs. 14O–AB)

1987 *Cruciplacolithus hayi* Covington and Wise, Pl. 1, Fig. 6.

1994 *Corollithion* cf. *C. achylosum* Bralower et al., Figs. 19.31, 19.32.

1997 *Crucibiscutum hayi* Aguado et al., Figs. 8.23, 8.24.

Derivation of name: From the Latin word *gracilis* meaning ‘slim’, ‘slender’, ‘delicate’, referring to the narrow rim and slim axial cross of this species.

Diagnosis: Small (3.4–4.7 μm) sub-circular to broadly elliptical (axial ratio ~1.1) *Crucibiscutum* coccoliths with a wide central area spanned by slim axial cross bars. The rim is narrow, bicyclic, with the bright inner cycle being usually slightly narrower (~0.5 μm width) than the outer dark cycle.

Journal Pre-proof

Description: The central area is wide (around twice as wide as the rim width) and partially covered by a slim bright cross with arms aligned with respect to the axes of the ellipse defined by the rim. The central cross is slightly brighter under XPL when oriented at 45º than when oriented to 0°.

Dimensions: L = 3.4–4.7 (average 4.1) μm; W = 3.2–4.4 (average 3.8) μm; specimens measured: 20.

Holotype: Figs. 14O, P [DG2808, DG2809] (are same specimen). Holotype dimensions: L = 4.4 μm, W = 4.2 μm.

Paratypes: Figs. 14Q [DG2810]; Figs. 14R, S [DG2811, DG2812] (are same specimen).

Type level: Uppermost Barremian, sample X.HA-2 [DGF001] (NC6A1) nannofossil Subzone; upper part of the *Imerites giraudi* AZ.

Type locality: X.HA section, Province of Granada, southeastern Spain.

Occurrence: Found throughout the upper Barremian to lower Aptian (uppermost part of the NC5E1 to NC6A2 CNSzs; lower part of the *Gassendiceras alpinum* ASz to *Hedbergella excelsa* Zone of planktonic foraminifera) in sections X.Cp_2, X.F, XF1, X.HA, X.Kv, X.Kv_2, and RA03 from the Subbetic Domain in the Betic Cordillera (southern Spain). This species was also recorded, as *Cruciplacolithus hayi*, in DSDP Site 603 off Cape Hatteras by Covington and Wise (1987) and as *Corollithion* cf. *C. achylosum* across the upper Barremian-lowermost Aptian of the ODP Site 641 by Bralower et al (1994).

Remarks: *Crucibiscutum gracile* differs from all previously described Neocomian *Crucibiscutum* species (*C. giraudii*, *C. neuquenensis*, *C. pinnatus*, *C. ryazanicum*, *C. salebrosum*, *C. trilensis*) including *C. bastetanum* (above) by having a wider central area and a narrower rim with a lower axial ratio (~ 1.1), usually showing a sub-circular outline. *Crucibiscutum gracile* also differs from *C. bastetanum*, *C. trilensis*, and *C.*

ryazanicum in having an axial slim cross spanning the central area. *Crucibiscutum gracile* has lower axial ratio and a wider and open central area than *C. pinnatus*. *Crucibiscutum hayi*, from the Upper Albian, has a greater axial ratio, a wider rim and a central area slightly narrow than that of *C. gracile*.

Family Cretarhabdaceae Thierstein, 1973

Genus *Flabellites* Thierstein, 1973

Flabellites oblongus (Buky, 1969) Crux in Crux et al., 1982

Remarks: A known morphological trend for the specimens of *Flabellites oblongus* along the upper Barremian–Albian (e.g., Aguado et al., 1997; Bown, 2005) is the increase in coccolith size. Recently, de Kaenel et al. (2020) erected a new species (*Flabellites eclepensensis*) for those small (3 to <5 µm) specimens previously assigned to *F. oblongus* (e.g., Aguado et al., 2014a). However, the mixture analysis performed in the present study (Chapter 4.1 and Fig. 8) suggest a rather continuous increase in size of the measured population. The selected size of 5 µm by de Kaenel et al. (2020) to separate the specimens assigned to *F. eclepensensis* within the complete pool of *F. oblongus* s.l. seems arbitrary. In the absence of any other distinctive biometric (e.g., ellipticity) or morphological character that could help in a net separation of both species, we opted here to retain the wide concept (*F. oblongus* s.l., or simply *F. oblongus*) of the species.

Order Eiffellithales Rood et al, 1971

Family Chiastozygaceae Rood et al., 1973

Genus *Chiastozygus* Gartner, 1968

Chiastozygus lamprostauros sp. nov.

Journal Pre-proof

PFNR: PFN001011.

(Figs. 14AC–AP)

1997 *Chiastozygus* sp. cf. *C. litterarius* Aguado et al., Figs. 15, 16.

2014a *Chiastozygus litterarius* Aguado et al., Figs. 3.1–3.3.

Derivation of name: From the Greek words *lampros* meaning 'bright', and *stauros* meaning 'cross', 'saltire', referring to the XPL image of this species.

Diagnosis: Small to medium-sized (4.3–7.2 μm) normally elliptical *Chiastozygus* coccoliths with a narrow (~1.2 μm) rim. The relatively wide central area is covered by a diagonal cross whose arms are seen simple and brighter than the rim when the longitudinal direction is oriented at 45° under XPL.

Description: This species has an axial ratio ~1.4 and a relatively narrow rim, which is dark and diffusely bicyclic under XPL. The diagonal cross spanning the central area have narrow (~0.5 μm) arms that show median lines and remain dark when the longitudinal direction is oriented at 0°. These arms are seen simple (without median lines) and bright under XPL when the longitudinal direction is oriented at 45°. The angle between the arms of the cross is greater (~105°) in the longitudinal direction than in the transverse direction (~75°). The arms of the diagonal cross are asymmetrical (slightly rotated) with respect to the axes of the ellipse. In some specimens, the diagonal cross supports the base of a distal stem.

Dimensions: L = 4.3–7.2 (average 5.6) μm; W = 3.4–5.5 (average 4.2) μm; specimens measured: 20.

Holotype: Figs. 14AC, AD [DG2813, DG2814] (are same specimen). Holotype dimensions: L = 6.2 μm, W = 5.0 μm.

Paratypes: Figs. 14AE, AF [DG2815, DG2816] (are same specimen); Figs. 14AL, AM [DG2817, DG2818] (are same specimen).

Type level: Uppermost Barremian, sample X.HA-7 [DGF002] (NC6A2 CNSz; *Martelites sarasini* AZ).

Type locality: X.HA section, Province of Granada, southeastern Spain.

Occurrence: Found, as a rare species, from the upper Barremian (upper part of the NC5E2 CNSz, *Gerhardtia provincialis* ASz) to uppermost lower Aptian (NC7A2 CNSz, *Schackoina cabri* Zone of planktonic foraminifera). Recorded in sections X.Cp_2, X.F, X.F1, X.HA, X.Kv, X.Kv_2, and RA03 from the Subbetic Domain in the Betic Cordillera (southern Spain).

Remarks: *Chiastozygus lamprostauros* is rather similar to *Chiastozygus amphipons* (Santonian–Maastrichtian) in rim construction and optical behavior from which is differentiated by having the arms of the diagonal cross slightly rotated with respect to the axes of the ellipse (asymmetric). It differs from *Chiastozygus bifarius* (Albian–Maastrichtian) and *Chiastozygus platyrhethus* (Aptian–Coniacian) by having a narrower, simple (with no median lines when oriented at 45°) diagonal cross with slightly asymmetrical (rotated) arms with respect to the axes of the ellipse. *Chiastozygus litterarius* (Aptian–Maastrichtian) is a rather poorly documented taxon originally described from the upper Maastrichtian sedimentary successions of Poland, and is characterized by having a weakly birefringent diagonal cross instead of the bright cross when oriented at 45° which is present in *C. lamprostauros*. *Chiastozygus tenuis* (another poorly documented species) has a slim diagonal cross symmetrical with respect of the axes of the ellipse instead of a broader, slightly rotated one as present in *C. lamprostauros*. *Chiastozygus lamprostauros* differs from other species of this genus (*C. antiquus*, *C. garrisoni*, *C. stylesii* and *C. trabalis*) by having a dark diffusely bicyclic

rim. Probably most of the late Barremian–early Aptian *C. litterarius* specimens from the literature should be assigned to *C. lamprostauros*.

Family Rhagodiscaceae Hay, 1977

Genus *Rhagodiscus* Reinhardt, 1967

Rhagodiscus sicutclipeus sp. nov.

PFNR: PFN001009.

(Figs. 14AQ–BD)

2014a *Rhagodiscus* sp. cf. *R. achlyostaurion* Aguado et al., Figs. 3.48–50.

2014b *Rhagodiscus* sp. cf. *R. achlyostaurion* Aguado et al., Fig. 3.3.

Derivation of name: From the Latin words *sicut* meaning 'as', 'such as', and *clipeus*, the elliptical war shield used by the ancient Greeks and Romans which resembles the XPL image of this species.

Diagnosis: Small to medium-sized (4.6–5.9 μm) normally elliptical *Rhagodiscus* coccoliths with a relatively wide central area bearing a small spine base, which is bright in XPL. The rim and central area images are distinctly dark in XPL.

Description: This species has an elliptic rim (axial ratio ~1.4) and central area that remain relatively dark under XPL. The central area bears a small spine base, which is seen as a bright, solid (not hollow) circle traversed by four sharp extinction gyres. The spine base is relatively small (~1.3 μm in diameter), remains isolated in the middle of the central area and does not reach the internal margin of the rim.

Dimensions: L = 4.6–5.9 (average 5.1) μm; W = 3.3–4.6 (average 3.7) μm; specimens measured: 20.

Holotype: Fig. 14AQ [DG2819]. Holotype dimensions: L = 5.3 μm, W = 3.7 μm.

Paratypes: Figs. 14AR, AS [DG2820, DG2821].

Type level: Upper Barremian, sample X.HA-4 [DGF003] (NC6A1 CNSz; *Martelites sarasini* AZ).

Type locality: X.HA section, Province of Granada, southeastern Spain.

Occurrence: Found, as a rare species, from the upper Barremian (upper part of the NC5E2 CNSz, *Gerhardtia sartousiana* ASz) to uppermost lower Aptian (NC7A2 CNSz, *Deshayesites forbesi* AZ). Recorded in sections X.Ag_6, X.Cp_2, X.F, X.F1, X.HA, X.Kv, X.Kv_2, and RA03 from the Subbetic Domain in the Betic Cordillera (southern Spain).

Remarks: *Rhagodiscus sicutclipeus* is rather similar to *Rhagodiscus achlyostaurion* (upper Aptian–Coniacian) from which differs by its noticeably smaller central spine base, which does not seem hollow and does not reach the internal margin of the rim. *Rhagodiscus pancostii* (Lower Turonian) is smaller in size (holotype length = 3.96 μm) and lacks the distinctly optical features present in the rim and central area of *R. sicutclipeus*. *Rhagodiscus hamptonii* (upper Aptian–Upper Albian) is greater in size and has a less clearly defined (usually absent) bright spine base. *Rhagodiscus buisensis* lacks the solid birefringent spine base (de Kaenel et al., 2020) present in *R. sicutclipeus*. Probably most of the Barremian–lower Aptian occurrences of *R. achlyostaurion* cited in the literature correspond to *R. sicutclipeus*.

Order Watznaueriales Bown, 1987

Family Watznaueriaceae Rood et al., 1971

Genus *Cyclagelosphaera* Noël, 1965

Cyclagelosphaera platyaspis sp. nov.

PFNR: PFN001010.

Journal Pre-proof

(Figs. 12N–Q)

Derivation of name: From the Greek words *platys*, meaning 'wide' and *aspis* meaning 'shield', alluding to the wider distal shield of this species.

Diagnosis: Medium to large-sized (7.0–8.4 μm) *Cyclagelosphaera* coccoliths having a wide distal shield and a very small (1.1–1.4 μm) central area.

Description: Circular placoliths with proximal and distal shield elements composed by R-units. In distal view, the V-unit forms a narrow distal cycle around the central area and is seen as a thin, dark line under XPL. The central area is very small (1.1–1.4 μm) compared to the distal shield (7.0–8.4 μm), and is completely closed.

Dimensions: W = 7.0–8.4 (average 7.5) μm; specimens measured: 6.

Holotype: Fig. 12N [DG2827]. Holotype dimensions: W = 8.4 μm, central area = 1.1 μm.

Paratypes: Figs. 12O, P, Q [DG2828, DG2829, DG2847].

Type level: Uppermost Barremian, sample X.Kv$_2$-700 [DGF004] (NC6A2 CNSz; lower part of the *Martelites sarasini* AZ).

Type locality: X.Kv$_2$ section, Province of Murcia, southeastern Spain.

Occurrence: Sporadically recorded throughout the upper Barremian to lowermost Aptian (uppermost part of the *Gassendiceras alpinum* ASz to the *Deshayesites oglanlensis* AZ). This interval is equivalent to the uppermost part of the NC5E1–NC6A2 CNSzs. This species is a very rare component of the assemblages. It has been recorded from sections X.Kv, X.Kv$_2$ and X.Ag$_6$ in the Subbetic Domain of the Betic Cordillera (southern Spain).

Remarks: *Cyclagelosphaera platyaspis* differs from *Cyclagelosphaera margerelii* by having a noticeably larger size (7.0–8.4 μm instead of 4–6 μm), although both species

have a very small central area closed by calcite elements. *Cyclagelosphaera platyaspis* differs from *Cyclagelosphaera brezae* by having a distinct V-unit cycle around the central area, and from *C. argoensis*, *C. jiangii*, *C. lacuna* and *C. wiedmannii* by the lack of central opening or open central area. *Cyclagelosphaera rotaclypeata* and *C. deflandrei* both have central areas wider than that of *C. platyaspis*, which also lacks the raised central plugs present in *C. reinhardtii* and *C. shenleyensis*.

Nannoliths *Incertae sedis*

Family Microrhabdulaceae Deflandre, 1963

Genus *Lithraphidites* Deflandre, 1963

Lithraphidites aichmoides sp. nov.

PFNR: PFN001012.

(Figs. 12A–H)

Derivation of name: From the Greek words *aichme* meaning 'spearhead', and the suffix *-oides* meaning 'resembling'.

Diagnosis: Very large (15.3–25.3 μm) *Lithraphidites* nannolith having an outline similar to a bladed dagger. In the direction opposite to the 'handle', the outline is slightly convex and decreases its width slowly before tapering toward the point. The maximum width oscillates between 2.7 and 4.1 μm.

Description: Calcareous rods with cruciform cross-section built of long blades of identical optical orientation. The outline is similar to a bladed dagger in which the 'handle' (~1.1 μm width and frequently missing by breakage) is followed by a wider expansion (2.7–4.1 μm width) which slowly decreases its width before tapering toward the point.

Journal Pre-proof

Dimensions: L = 15.3–25.3 (average 19.6) μm; W = 2.7–4.1 (average 3.6) μm; specimens measured: 30.

Holotype: Fig. 12A [DG2822]. Holotype dimensions: L = 20.1 μm, W = 3.2 μm.

Paratypes: Figs. 12B–D [DG2823–DG2825], H [DG2826].

Type level: Uppermost Barremian, sample X.Kv_2-235 [DGF005] (NC5E2 CNSz; lowermost part of the *Gerhardtia sartousiana* ASz).

Type locality: X.Kv_2 section, Province of Murcia, southeastern Spain.

Occurrence: Recorded from the uppermost lower Barremian (upper part of the *Moutoniceras moutonianum* AZ) to the upper Barremian (uppermost part of the *Hemihoplites feraudianus* ASz), within NC5E1–NC6A1 CNSzs. This species is a rare component of the assemblages, but has a consistent and continuous record until the uppermost part of the *Gerhardtia provincialis* ASz. It has been recorded from sections X.CO_2, X.CT, X.F, X.Kv, X.Kv_2, and X.V_1 from the Subbetic Domain in the Betic Cordillera (southern Spain). The LO of *L. aichmoides* has been recorded 467 cm above that of *Flabellites oblongus* (base of NC5E1 CNSz) in section X.V_1.

Remarks: *Lithraphidites aichmoides* differs from *L. magnus* (emend.) and *L. pugio* by having a more stylized outline, with a maximum width smaller than 4.5 μm. This width appears as the more appropriate to separate both species according to the measurements made in the present study (Fig. 5). *Lithraphidites aichmoides* differs from *Lithraphidites alatus* (Upper Albian–Lower Cenomanian) by having an outline similar to a bladed dagger instead of a 'closed umbrella', the latter decreasing quickly in width from the end close to the 'handle' towards the point. It differs from *Lithraphidites houghtonii* (Boreal lower–upper Aptian) by having a greater length and a smaller width.

Lithraphidites magnus (Covington and Wise, 1987) comb. & stat. nov.

PFNR: PFN001015.

(Figs. 13F–J)

1987 *Lithraphidites alatus* ssp. *magnus* Covington and Wise, Pl. 10, Figs. 3, 4, 8?.

1994 *Lithraphidites alatus* ssp. *magnus* Bralower et al., Figs. 20.7, 20.8.

2020 *Lithraphidites magnus* Martinez et al., Fig. 4M.

Emended diagnosis: Very large (usually >21 μm) *Lithraphidites* nannolith having an outline similar to a bladed dagger. The 'handle' (~1.1 μm width and sometimes missing by breakage) is followed by a wider expansion (4.5–7.0 μm width) which nearly maintains its width a long distance (around three fifths of the nannolith length) before tapering toward the point. The maximum width is greater than 4.5 μm and the L/W ratio is greater than 3.5 (average 4.1).

Remarks: Covington and Wise (1987, p. 631) originally described this taxon, but as a subspecies of *Lithraphidites alatus* (*L. alatus* ssp. *magnus*). *Lithraphidites magnus* is here erected to the category of species because the lack of stratigraphic connection with *L. alatus* and the existence of morphologic differences between both taxa. While *L. magnus* is restricted to the uppermost Barremian–lowermost Aptian, *L. alatus* ranges from Upper Albian to Lower Cenomanian. The original description of *L. magnus* was based on two SEM micrographs in which specimens are foreshortened due to tilting or partially covered. The estimated holotype dimensions were 5.7 μm width and ~20 μm long. However, the holotype appears to be a broken specimen, its true length probably being ~25 μm. The length in the population measured in the present paper oscillates between 21.2 and 26.2 μm (average 23.8 μm). After a biometric study (Fig. 6), all specimens with L/W ratio smaller than 3.7 (usually with L<21 μm) were here assigned to *Lithraphidites pugio* n. sp., which is characterized by a wider and shorter outline (see

below). It seems a width greater than 4.5 μm is also a good value to characterize these forms differentiating them from *Lithraphidites aichmoides* n. sp. (Fig. 5).

Occurrence: Covington and Wise (1987) recorded this taxon in sediments from core 44 of DSDP Hole 603B (North American Basin of North Atlantic). These were dated as lower Aptian, although no convincing evidence supporting this age was provided from calcareous nannofossil assemblages. Bralower et al. (1994) reported this species from upper Barremian–lower Aptian sediments of DSDP Site 398 (West Iberian continental margin). Cobianchi et al. (1997) recorded this species throughout upper Barremian–lower Aptian (*M. hoschulzii* to *H. irregularis* CNZs) in northern Gargano (Apulia, Italy). However, the species concept of these authors probably includes *L. magnus* and *L. pugio* as differentiated here, which originates an expanded range. In the Subbetic Domain of the Betic Cordillera, *L. magnus* has been recorded from the uppermost Barremian (uppermost part of the *Heteroholcoplites feraudianus* ASz) to the lower Aptian (lower part of the *Deshayesites forbesi* AZ), thoroughout most of the lowermost part of NC6A CNSz. This species is a rare component of the assemblages, but has a consistent and continuous record until the upper part of the *Martelites sarasini* AZ, from which it becomes rare. It has been recorded from sections X.Cp_2, X.F, X.F1, X.HA, X.Kv, X.Kv_2, and RA03, in the Subbetic Domain of the Betic Cordillera (southern Spain).

Lithraphidites pugio sp. nov.

PFNR: PFN001013.

(Figs. 12I–M; Figs. 13A–E)

2017 *Lithraphidites magnus* Aguado et al., Fig. 2.

2020 *Lithraphidites* sp. cf. *L. magnus* Martinez et al., Fig. 4N.

Derivation of name: From the Latin word *pugio*, the double-edged, straight short dagger used by the ancient Romans, whose outline resembles that of this species.

Diagnosis: Very large (13.4–23.5 μm) *Lithraphidites* nannolith having an outline similar to a short bladed dagger. In the direction opposite to the 'handle', the outline is convex and quickly decreases its width before tapering toward the point. The maximum width oscillates between 4.5 and 8.1 μm.

Description: Calcareous rods with cruciform cross-section built of long blades of identical optical orientation. The outline is similar to a bladed dagger in which the 'handle' (~1.1 μm width and frequently missing by breakage) is followed by a wider expansion (4.5–8.1 μm width) which nearly maintains its width a short distance (around a half of the nannolith length) before quickly tapering toward the point. The L/W ratio is smaller than 3.5 (average 2.9).

Dimensions: L = 13.4–23.5 (average 18.1) μm; W = 4.5–8.1 (average 6.2) μm; specimens measured: 48.

Holotype: Fig. 12I [DG2842]. Holotype dimensions: L = 19.6 μm, W = 7.8 μm.

Paratypes: Figs. 12K, L, [DG2843, DG2844]; *Lithraphidites* sp. cf. *L. magnus* in Martinez et al., 2020; Fig. 4N, which is reproduced here as Fig. 13A, [DG2845]; Fig. 13B, [DG2846].

Type level: Uppermost Barremian, sample X.Kv$_2$-228 [DGF006] (NC5E2 CNSz; lowermost part of the *Gerhardtia sartousiana* ASz).

Type locality: X.Kv$_2$ section, Province of Murcia, southeastern Spain.

Occurrence: In the Subbetic Domain of the Betic Cordillera, *L. pugio* has been recorded throughout part of the upper Barremian (from the middle part of the *Gassendiceras alpinum* ASz to the uppermost part of the *Hemihoplites feraudianus* ASz; base of NC5E2 to basal part of NC6A1 CNSzs). This species is scarce, but has a consistent

Journal Pre-proof

record in the assemblages from the X.F, X.HA, X.Kv, X.Kv_2 and X.V_1 sections. Martinez et al. (2020) used the LO of this species to correlate the uppermost part of the X.V_1 and the lowermost part of the X.Kv_2 sections. This bioevent has shown biostratigraphic potential to be used in correlation, at least at a regional scale (chapters 5.1 and 5.2).

Remarks: *Lithraphidites pugio* differs from *L. magnus* (emend.) by having a shorter (usually < 21 μm) and wider outline, with an average L/W ratio ~2.9. The expansion of the blades decreases more quickly in *L. pugio* than in *L. magnus*. It differs from *L. aichmoides* by having a greater width (>4.5 μm) and nearly parallel sides (by around the half of its length) in side view, before tapering at the end. *Lithraphidites pugio* differs from *Lithraphidites alatus* (Upper Albian–Lower Cenomanian) by having an outline similar to a short bladed dagger instead of a 'closed umbrella', the latter having a straight to slightly concave outline quickly decreasing in width from the end close to the 'handle' towards the point. Jeremiah (2001) described *Lithraphidites houghtonii* from the lower–upper Aptian transition (*Deshayesites forbesi* to *Epicheloniceras martinoides* AZs) of the Central North Sea. This later species is morphologically rather similar to *L. pugio*, from which it differs in having a smaller size (length = 9–12 μm, width ~5.6 μm).

Radiate multielement group

Genus *Hayesites* Manivit, 1971

Hayesites irregularis E

(Figs. 15A–R)

2020 *Hayesites irregularis* E Martinez et al., Figs. 4I–L.

Journal Pre-proof

Diagnosis: Specimens of *H. irregularis* (Thierstein in Roth and Thierstein, 1972) Applegate et al. in Covington and Wise, 1987 with an elongated outline (L/W>1.12) usually showing poorly defined radial elements under cross-polarized light microscopy (XPL). See section 4.2 for details.

Description: A mixture analysis performed on the L/W ratio of 140 specimens of the *H. irregularis* gr. (Fig. 7C and SM2) indicates that two populations are present within this pool. Those forms with nearly circular outline, (L/W smaller or equal to 1.12), being younger in time, were assigned to *Hayesites irregularis* s.str. These specimens having a more elongated outline (L/W>1.12), generally showing poorly defined radial elements and being slightly older, were assigned to *H. irregularis* morphotype E (*H. irregularis* E).

Dimensions: L = 2.8–5.3 (average 3.8) μm; W = 2.2–4.3 (average 3.0) μm; specimens measured: 51.

Occurrence: *Hayesites irregularis* E was recorded from the lower part of the *Hemihoplites feraudianus* ASz in the Subbetic Domain of the Betic Cordillera (sections RA03, X.Ag$_6$, X.F, X.HA, X.Kv, X.Kv$_2$) and extends throughout the *Imerites giraudi*–*Deshayesites oglanlensis* AZs of the upper Barremian–lowermost Aptian. The LO of this species has been used here to define the base of the NC6A1 CNSz. The LO of *H. irregularis* s. str. was recorded from the middle part of *I. giraudi* AZ.

Nannoliths

Order Braarudosphaerales Aubry, 2013 emend. Lees and Bown, 2016

Family Nannoconaceae Deflandre, 1959

Genus *Nannoconus* Kamptner, 1931

Nannoconus sp. cf. *N. truittii*

Journal Pre-proof

(Figs. 15AK–AM)

Diagnosis: Specimens of *Nannoconus* resembling *N. truittii* ssp. *rectangularis* Dères and Achéritéguy, 1980 in being wider than tall in side view and having a central canal of similar width than the wall. They differ from *N. truittii* ssp. *rectangularis* by showing a slightly conical, instead of rectangular, outline.

Dimensions: L = 5.6–9.9 (average 7.4) μm; W = 8.1–11.9 (average 10.2) μm; specimens measured: 28.

Occurrence: These forms were recorded (Figs. 3, 4; sections RA03, X.Ag6, X.CP_2, X.F, X.F1, X.HA, X.Kv, X.Kv_2) from the upper part of the *Nemihoplites feraudianus* ASz to the *Deshayesites forbesi* AZ (NC6A1–NC6A2 CNSz).

Remarks: *Nannoconus truittii* ssp. *frequens* and *N. truittii* ssp. *truittii* are respectively taller than wide and of similar height than width in side view (Brönnimann, 1955; Dères and Achéritéguy, 1980), differing from *N.* sp. cf. *N. truittii*. *Nannoconus truittii* ssp. *rectangularis* was described from the Albian (Dères and Achéritéguy, 1980), while *N.* sp. cf. *truittii* has been recorded form the uppermost Barremian–lower Aptian.

7. Conclusions

A detailed study of the calcareous nannofossil assemblages from twelve uppermost lower Barremian–lowermost Aptian sections in the Subbetic Domain of the Betic Cordillera, well dated by ammonite biostratigraphy, has allowed to the identification of seven new species. The new taxa *Crucibiscutum bastetanum*, *Crucibiscutum gracile*, *Chiastozygus lamprostauros*, *Cyclagelosphaera platyaspis*, *Lithraphidites aichmoides*, *Lithraphidites pugio*, and *Rhagodiscus sicutclipeus* are described, one species is

emended (*Lithraphidites magnus*) and the taxonomic concept of the marker species *Hayesites irregularis* is discussed and clarified.

The stratigraphic ranges of each new species, together with those of other relevant markers, are directly correlated to standard ammonite biostratigraphy and tied to the geochronological scale using a previous astrochronological calibration of the complete interval studied.

Five new calcareous nannofossil subzones are proposed (NC5E1, NC5E2, NC5E3, NC6A1, and NC6A2) which allow the refinement of the zonation for the Mediterranean–Atlantic Province of the Tethyan Realm and are directly correlated with respect to the standard Tethyan ammonite zonation. Two of the new species described here are used as biostratigraphic markers for the new proposed subzones. The duration of each one of these subzones is also provided through a previous astrochronological calibration.

The implications of these results on the extant definition of the Barremian/Aptian boundary are discussed. In the absence of magnetostratigraphic data, we chose the definition of the Barremian/Aptian boundary in coincidence with the LO of the ammonite species *Deshayesites oglanlensis*. Regarding calcareous nannofossils, none of the biostratigraphic reliable markers coincides with this boundary. The recorded bioevent closer to the Barremian/Aptian boundary was the HO of the new species *Crucibiscutum bastetanum*, which correlates to the lower part of the *Martelites sarasini* AZ. Based on its proximity to the base of the *D. oglanlensis* AZ, the ISNE of the $\delta^{13}C$

Journal Pre-proof

curve may be an alternative for the definition of the base of the Aptian, if it is identified in additional locations.

The morpho-evolutionary trends and paleogeographic distribution of some selected nannofossil taxa (mainly from genera *Flabellites*, *Lithraphidites* and *Micrantholithus*) across the interval studied were analyzed. This analysis suggests that paleogeography played a fundamental role as a factor controlling the evolution of the calcareous nannoplankton in the west European-Atlantic region during the late Barremian–early Aptian interval.

The following are the supplementary data related to this article.

Supplementary Material 1 (SM1): Detailed location, lithostratigraphy and previous data on biostratigraphy of the sections studied.

Supplementary Material 2 (SM2): a) stratigraphic ranges of individual calcareous nannofossil species in the 12 sections studied; b) size measurements of the new species described and the additional taxa included in the biometric study.

Supplementary Material 3: Alphabetic list of all taxa cited in the text, with author attributions and dates.

Acknowledgements

We want to express our gratitude to M.J. Campos, who helped with the processing of smear slides. This study was funded by research projects P20_00783 (Plan Andaluz de Investigación, Desarrollo e Innnovación), CGL2014-52546-P (Ministerio de Ciencia, Innovacíon y Universidades, Spain) and RNM-200 Research Group (Junta de Andalucía, Spain). This study was designed by RA, who performed the calcareous

Journal Pre-proof

nannofossil study, wrote the initial draft, and elaborated the figures. All the authors collected the samples in the field. MC and JS provided the ammonite data, and MM the astrochronological calibration. The authors are very grateful to F. Giraud and J. Mutterlose, whose constructive comments led to improvements in the final version of this paper, and to R. Jordan for his helpful editorial assistance.

Author_statement

Roque Aguado: Conceptualization, Methodology, Validation, Formal analysis, Resources, Data Curation, Writing – Original Draft, Writing – Review & Editing, Visualization, Supervision, Funding acquisition. **Miguel Company**: Investigation, Resources, Writing – Review & Editing. **Luis O'Dogherty**: Resources, Writing – Review & Editing, Funding acquisition. **José Sandoval**: Investigation, Resources, Writing – Review & Editing. **Mathieu Martinez**: Resources, Writing – Review & Editing.

Delaration of competing interest

None.

References

Aguado, R., 1994. Nannofósiles del Cretácico de la Cordillera Bética. Bioestratigrafía, PhD Thesis. Dpt. Estratigrafía y Paleontología y Servicio de publicaciones de la Universidad de Granada, Granada, 413 pp.

Aguado, R., Castro, J.M.I., Company, M., de Gea, G.A., 1999. Aptian bioevents — an integrated biostratigraphic analysis of the Almadich Formation, Inner Prebetic Domain, SE Spain. Cretaceous Research 20, 663–683. https://doi.org/10.1006/cres.1999.0176.

Aguado, R., Company, M., Martinez, M., Martínez-López, F.J., O'Dogherty, L., Sánchez-Bellón, A., Sandoval, J., 2017. Bioestratigrafía de alta precisión del Barremiense mediterráneo mediante nanofósiles calcáreos, in: O'Dogherty, L.C.

Journal Pre-proof

(Ed.). XXXIII Jornadas de Paleontología, Cádiz, Spain, 27–30 Septiembre. Libro de Resúmenes, pp. 11–15.

Aguado, R., Company, M., O'Dogherty, L., Palomo, I., Sandoval, J., Tavera, J.M., 2008. Análisis estratigráfico integrado del Hauteriviense terminal–Barremiense inferior de la sección de Arroyo Gilico (Murcia), in: Ruiz-Omeñaca, J.I., Piñuela, L., et al. (Eds.), XXIV Jornadas de la Sociedad Española de Paleontología, Libro de resúmenes, Colunga, Asturias, pp. 59–60.

Aguado, R., Company, M., O'Dogherty, L., Sandoval, J., Tavera, J.M., 1992. Biostratigraphic analysis of the pelagic Barremian/Aptian in the Betic Cordillera (southern Spain). Preliminary data. Cretaceous Research 13, 445–452. https://doi.org/10.1016/0195-6671(92)90009-f.

Aguado, R., Company, M., O'Dogherty, L., Sandoval, J., Tavera, J.M., 2014a. Late Hauterivian–early Barremian calcareous nannofossil biostratigraphy, palaeoceanography, and stable isotope record in the Subbetic Domain (southern Spain). Cretaceous Research 49, 105–124. https://doi.org/10.1016/j.cretres.2014.02.006.

Aguado, R., Company, M., Sandoval, J., Tavera, J.M., 1997. Biostratigraphic events at the Barremian/Aptian boundary in the Betic Cordillera (southern Spain). Cretaceous Research 18, 309–329. https://doi.org/10.1006/cres.1997.0069.

Aguado, R., de Gea, G.A., Castro, J.M., O'Dogherty, L., Quijano, M.L., Naafs, B.D.A., Pancost, R.D., 2014b. Late Barremian–early Aptian dark facies of the Subbetic (Betic Cordillera, southern Spain): Calcareous nannofossil quantitative analyses, chemostratigraphy and palaeoceanographic reconstructions. Palaeogeography, Palaeoclimatology, Palaeoecology 395, 198–221. https://doi.org/10.1016/j.palaeo.2013.12.031.

Aguado, R., de Gea, G.A., O'Dogherty, L., 2014c. Integrated biostratigraphy (calcareous nannofossils, planktonic foraminifera, and radiolaria) of an uppermost Barremian–lower Aptian pelagic succession in the Subbetic Basin (southern Spain). Cretaceous Research 51, 153–173. https://doi.org/10.1016/j.cretres.2014.06.002.

Akaike, H., 1974. A new look at the statistical model identification, IEEE Transactions on Automatic Control 19, 716–723. https://doi.org/10.1109/TAC.1974.1100705.

Applegate, J.L., Bergen, J.A., Covington, J.M., Wise, S.W., Jr., 1989. Lower Cretaceous calcareous nannofossils from continental margin drill sites off North Carolina (DSDP Leg 93) and Portugal (ODP Leg 103): a comparison, in: Crux, J.A., Van-Heck, S.E. (Eds.), Nannofossils and their applications. British Micropalaeontological Society Publication Series. Ellis Horwood Ltd., Chichester, pp. 212–222.

Baccelle, L., Bosellini, A., 1965. Diagrammi per la stima visiva della composizione percentuale nelle rocce sedimentarie. Annali dell'Università di Ferrara Sezione IX 1/3, 59–62.

Barrier, E., Vrielynck, B., Brouillet, J.-F., Brunet, M.-F., 2018. Paleotectonic Reconstruction of the Central Tethyan Realm, CCGM-CGMW, Paris.

Barron, E.J., Harrison, C.G.A., Sloan II, J.L., Hay, W.W., 1981. Paleogeography, 180 million years ago to the present. Eclogae Geologicae Helvetiae 74, 443–470.

Bellanca, A., Erba, E., Neri, R., Premoli-Silva, I., Sprovieri, M., Tremolada, F., Verga, D., 2002. Palaeoceanographic significance of the Tethyan 'Livello Selli ' (Early Aptian)from the Hybla Formation, northwestern Sicily: biostratigraphy and high-resolution chemostratigraphic records. Palaeogeography, Palaeoclimatology, Palaeoecology 185, 175–196. https://doi.org/10.1016/s0031-0182(02)00299-7.

Journal Pre-proof

Bollmann, J., Klaas, C., 2008. Morphological variation of *Gephyrocapsa oceanica* Kamptner 1943 in plankton samples: implications for ecologic and taxonomic interpretations. Protist 159, 369–381.

Bollmann, J., Herrle, J.O., Cortés, M.Y., Fielding, S.R., 2009. The effect of sea water salinity on the morphology of *Emiliania huxleyi* in plankton and sediment samples. Earth and Planetary Science Letters 284, 320–328.

Bornemann, A., Mutterlose, J., 2006. Size analyses of the coccolith species *Biscutum constans* and *Watznaueria barnesiae* from the Late Albian "Niveau Breistroffer" (SE France): taxonomic and palaeoecological implications. Geobios 39, 599–615. https://doi.org/10.1016/j.geobios.2005.05.005.

Bottini, C., Mutterlose, J., 2012. Integrated stratigraphy of Early Aptian black shales in the Boreal Realm: calcareous nannofossil and stable isotope evidence for global and regional processes. Newsletters on Stratigraphy 45, 115–137. https://doi.org/10.1127/0078-0421/2012/0017.

Bown, P.R., 1998. Calcareous Nannofossil Biostratigraphy. British Micropalaeontological Society Publication Series, 1 ed., Chapman and Hall, London, 314 pp.

Bown, P.R., 2005. Early to mid-Cretaceous calcareous nannoplankton from the Northwest Pacific Ocean, Leg 198, Shatsky Rise, in: Bralower, T.J., Premoli-Silva, I., et al. (Eds.), Proceedings of the Ocean Drilling Program Scientific Results 198, pp. 1–82.

Bown, P.R., Young, J.R., 1997. Mesozoic calcareous nannoplankton classification. Journal of Nannoplankton Research 19, 21–36.

Journal Pre-proof

Bown, P.R., Young, J.R., 1998. Techniques, in: Bown, P.R. (Ed.), Calcareous Nannofossil Biostratigraphy. British Micropalaeontological Society Publication Series. Chapman and Hall, London, pp. 16–28.

Bown, P.R., Rutledge, D.C., Crux, J.A., Gallagher, L.T., 1998. Lower Cretaceous, in: Bown, P.R. (Ed.), Calcareous Nannofossil Biostratigraphy. British Micropalaeontological Society Publication Series. Chapman and Hall, London, pp. 86–131.

Bralower, T.J., Arthur, M.A., Leckie, M.A., Sliter, W.V., Allard, D.J., Schlanger, S.O., 1994. Timing and palaeoceanography of oceanic dysoxia/anoxia in the Late Barremian to Early Aptian (Early Cretaceous). Palaios Research Letters 9, 335–369.

Bralower, T.J., Leckie, R.M., Sliter, W.V., Thierstein, H.R., 1995. An integrated Cretaceous microfossil biostratigraphy, in: Berggren, W.A., Kent, D.V., et al. (Eds.), Geochronology, Time Scales and Global Stratigraphic Correlation. The Society of Economic Paleontologists and Mineralogists Special Publication 54 pp. 65–79.

Brönnimann, P., 1955. Microfossils incertae sedis from the Upper Jurassic and Lower Cretaceous of Cuba. Micropaleontology 1, 28–51. https://doi.org/10.2307/1484409.

Cao, W., Zahirovic, S., Flament, N., Williams, S., Golonka, J., Müller, R.D., 2017. Improving global paleogeography since the late Paleozoic using paleobiology. Biogeosciences 14, 5425–5439. https://doi.org/10.5194/bg-14-5425-2017.

Casey, R., Bayliss, H.M., Simpson, M.I., 1988. Observations on the lithostratigraphy and ammonite succession of the Aptian (Lower Cretaceous) Lower Greensand of Chale Bay, Isle of Wight, UK. Cretaceous Research 19, 511–535.

Castro, J.M., Ruiz-Ortiz, P.A., de Gea, G.A., Aguado, R., Jarvis, I., Weissert, H.J., Molina, J.M., Nieto, L.M., Pancost, R.D., Quijano, M.L., Reolid, M., Skelton, P.W., López Rodríguez, C., Martínez-Rodríguez, R., 2021. High-resolution C-isotope, TOC

and biostratigraphic records of OAE 1a (Aptian) from an expanded hemipelagic cored succession, western Tethys: a new stratigraphic reference for global correlation and paleoenvironmental reconstruction. Paleoceanography and Paleoclimatology. https://doi.org/10.1029/2020PA004004.

Channell, J.E.T., Erba, E., Muttoni, G., Tremolada, F., 2000. Early Cretaceous magnetic stratigraphy in the APTICORE drill core and adjacent outcrop at Cismon (Southern Alps, Italy), and correlation to the proposed Barremian-Aptian boundary stratotype. Geological Society of America Bulletin 112, 1430–1443. https://doi.org/10.1130/0016-7606(2000)112<1430:ECMSIT>2.0.CO;2.

Cobianchi, M., Luciani, V., Bosellini, A., 1997. Early Cretaceous nannofossils and planktonic foraminifera from northern Gargano (Apulia, southern Italy). Cretaceous Research 18, 249–293. https://doi.org/10.1006/cres.1996.0058.

Coccioni, R., Premoli-Silva, I., 1994. Planktonic foraminifera from the Lower Cretaceous of Río Argos sections (southern Spain) and biostratigraphic implications. Cretaceous Research 15, 645–687. https://doi.org/10.1006/cres.1994.1037.

Coccioni, R., Galeotti, S., Sprovieri, M., 2003. The Mid-Barremian Event (MBE): the prelude to the OAE1a. EOS Trans. AGU 84 (46), Abstract PP41B–0835.

Coccioni, R., Premoli-Silva, I., Marsili, A., Verga, D., 2007. First radiation of Cretaceous planktonic foraminifera with radially elongate chambers at Angles (Southeastern France) and biostratigraphic implications. Revue de Micropaléontologie 50, 215–224. https://doi.org/10.1016/j.revmic.2007.06.005.

Company, M., Sandoval, J., Tavera, J.M., 1992. Secuencias deposicionales en el Barremiense-Aptiense inferior de la Sierra del Corque (Cordillera Bética): consideraciones paleogeográficas. Revista de la Sociedad Geológica de España 5, 55–63.

Journal Pre-proof

Company, M., Sandoval, J., Tavera, J.M., 1995. Lower Barremian ammonite biostratigraphy in the Subbetic Domain (Betic Cordillera, southern Spain). Cretaceous Research 16, 243–256. https://doi.org/10.1006/cres.1995.1018.

Company, M., Sandoval, J., Tavera, J.M., 2003. Ammonite biostratigraphy of the uppermost Hauterivian in the Betic Cordillera (SE Spain). Geobios 36, 685–694. https://doi.org/10.1016/j.geobios.2002.12.001.

Covington, J.M., Wise, S.W., Jr., 1987. Calcareous nannofossil biostratigraphy of a Lower Cretaceous deep sea fan complex: Deep Sea Drilling Project Leg 93, Site 603, lower continental rise off Cape Hatteras, in: Hinte, J.E. v., S.W. Wise, J., et al. (Eds.), Initial Reports of the Deep Sea Drilling Project 93. U. S. Government Printing Office, Washington, pp. 617–660.

Crux, J.A., 1989. Biostratigraphy and palaeogeographical applications of Lower Cretaceous nannofossils from north western Europe, in: Crux, J.A., Heck, S.E.V. (Eds.), Nannofossils and their Applications. British Micropalaeontological Society Publication Series. Ellis Horwood Ltd., Chichester, pp. 143–211.

de Gea, G.A., 2004. Bioestratigrafía y eventos del Cretácico Inferior en las Zonas Externas de la Cordillera Bética. Ph.D. Thesis. Servicio de Publicaciones de la Universidad de Jaén, Jaén, 658 pp.

de Kaenel, E.P., Mojon, P.O., Pictet, A., 2020. New biostratigraphical data (calcareous nannofossils, ammonites) and Early to Late Barremian transition in the Urgonien Jaune facies and Marnes de la Russille complex of the Swiss Jura Mountains. Swiss Journal of Palaeontology 139:6. https://doi.org/10.1186/s13358-020-00209-5.

Delanoy, G., 1995. About some significant ammonites from the Lower Aptian (Bedoulian) of the Angles-Barrême area (South-East France), in: Cecca, F. (Ed.),

Proceedings of the 3rd Workshop on Early Cretaceous Cephalopods. Piobbico, July 1994. Memorie Descrittive della Carta Geologica d'Italia 51, 65–101.

Déres, F., Achéritéguy, J., 1980. Biostratigraphie des nannoconidés. Bulletin des Centres de Recherche Exploration-Production Elf Aquitaine 4, 1–53.

Erba, E., 2004. Calcareous nannofossils and Mesozoic oceanic anoxic events. Marine Micropaleontology 52, 85–106. https://doi.org/10.1016/j.marmicro.2004.04.007.

Erba, E. (compiler), Aguado, R., Avram, E., Baraboschkin, E.J., Bergen, J.A., Bralower, T.J., Cecca, F., Channell, J.E.T., Coccioni, R., Company, M., Delanoy, G., Erbacher, J., Herbert, T.D., Hoedemaeker, P.J., Kakabadze, M., Lereveld, H., Lini, A., Mikhailova, I.A., Mutterlose, J., Ogg, J.G., Premoli-Silva, I., Rawson, P.F., von Salis, K., Weissert, H.J., 1996. The Aptian Stage. Bulletin de l'Institut Royal des Sciences Naturelles de Belgique. Sciences de la Terre 66-SUPP., 31–43.

Erba, E., Bottini, C., Faucher, G., Gambacorta, G., Visentin, S., 2019. The response of calcareous nannoplankton to Oceanic Anoxic Events: The Italian pelagic record. Bollettino della Società Paleontologica Italiana 58, 51–71. https://doi.org/10.4435/BSPI.2019.08.

Erba, E., Bottini, C., Weissert, H.J., Keller, C.E., 2010. Calcareous nannoplankton response to surface water acidification around Oceanic Anoxic Event 1a. Science 329, 428–432. https://doi.org/10.1126/science.1188886.

Erba, E., Channell, J.E.T., Claps, M., Jones, C., Larson, R., Opdyke, B., Premoli-Silva, I., Riva, A., Salvini, G., Torricelli, S., 1999. Integrated stratigraphy of the Cismon APTICORE (Southern Alps, Italy): a "reference section" for the Barremian-Aptian interval at low latitudes. Journal of Foraminiferal Research 29, 371–391.

Journal Pre-proof

Erba, E., Watkins, D.K., Mutterlose, J., 1995. Campanian dwarf calcareous nannofossils from the Wodejebato Guyot, in: Haggerty, J.A., Premoli-Silva, I., et al. (Eds.), Proceedings of the Ocean Drilling Program Scientific Results 144, pp. 141–156.

Faucher, G., Erba, E., Bottini, C., Gambacorta, G., 2017. Calcareous nannoplankton response to the latest Cenomanian Oceanic Anoxic Event 2 perturbation. Rivista Italiana di Paleontologia e Stratigrafia 123, 159–176.

Föllmi, K.B., 2012. Early Cretaceous life, climate and anoxia. Cretaceous Research 35, 230–257. https://doi.org/10.1016/j.cretres.2011.12.005.

Frau, C., 2020. Stable carbon-isotope chemostratigraphy versus ammonite biostratigraphy: data from around the Barremian/Aptian boundary (Lower Cretaceous). Strata 2020, Série 2e 56, 1–31.

Frau, C., Bulot, L.G., Delanoy, G., Moreno Bedmar, J.A., Masse, J.-P., Tendil, A.J.B., Lanteaume, C., 2018. The Aptian GSSP candidate at Gorgo a Cerbara (Central Italy): an alternative interpretation of the bio-, litho- and chemostratigraphic markers. Newsletters on Stratigraphy 51, 311–326. https://doi.org/10.1127/nos/2017/0422.

Giraud, F., Pittet, B., Grosheny, D., Baudin, F., Lécuyer, C., 2018. The palaeoceanographic crisis of the Early Aptian (OAE 1a) in the Vocontian Basin (SE France). Palaeogeography, Palaeoclimatology, Palaeoecology 511, 483–505. https://doi.org/10.1016/j.palaeo.2018.09.014.

Giraud, F., Pittet, B., Mattioli, E., Audouin, V., 2006. Paleoenvironmental controls on the morphology and abundance of the coccolith *Watznaueria britannica* (Late Jurassic, southern Germany). Marine Micropaleontology 60, 205–225. https://doi.org/10.1016/j.marmicro.2006.04.004.

Godet, A., Bodin, S., Föllmi, K.B., Vermeulen, J., Gardin, S., Fiet, N., Adatte, T., Berner, Z., Stüben, D., Van de Schootbrugge, B., 2006. Evolution of marine stable

carbon-isotope record during the early Cretaceous: A focus on late Hauterivian and Barremian in the Tethyan realm. Earth and Planetary Science Letters 242, 254–271. https://doi.org/10.1016/j.epsl.2005.12.011.

Gollain, B., Mattioli, E., Kenjo, S., Bartolini, A., Reboulet, S., 2019. Size patterns of the coccolith *Watznaueria barnesiae* in the lower Cretaceous: Biotic versus abiotic forcing. Marine Micropaleontology. https://doi.org/10.1016/j.marmicro.2019.03.012.

Gradstein, F.M., Ogg, J.G., Schmitz, M.D., Ogg, G.M., (Eds.). 2020. The Geologic Time Scale 2020. Elsevier, Amsterdam, Netherlands, 1390 pp.

Hallam, A., 1992. Phanerozoic Sea Level Changes. Columbia University Press, New York, 266 p.

Hammer, Ø., Harper, D.A.T., 2006. Paleontological Data Analysis. Blackwell Publishing Ltd., pp. 35–37.

Hammer, Ø., Harper, D.A.T., Ryan, P.D., 2001. PAST: paleontological statistics software package for education and data analysis. Palaeontologia Electronica 4, 1–9.

Hardenbol, J., Thierry, J., Farley, M.B., Jacquin, T., de Graciansky, P.-C., Vail, P.R., 1998. Mesozoic and Cenozoic sequence and chronostratigraphic framework of European basins. The Society of Economic Paleontologists and Mineralogists Special Publication No. 60, 3–13.

Huck, S., Heimhofer, U., Immenhauser, A., Weissert, H.J., 2013. Carbon-isotope stratigraphy of Early Cretaceous (Urgonian) shoal-water deposits: Diachronous changes in carbonate-platform production in the north-western Tethys. Sedimentary Geology 290, 157–174. https://doi.org/10.1016/j.sedgeo.2013.03.016.

Jakubowski, M., 1987. A proposed Lower Cretaceous nannofossil zonation scheme for the Moray Firth area of the North Sea. Abhandlungen der Geologischen Bundes-Anstalt 39, 99–119.

Journal Pre-proof

Janin, M.C., 1998. Remarques sur l'ultrastructure et les affinités biologiques des *Lithraphidites*, nannofossiles calcaires du Crétacé. Revue de Micropaléontologie 41, 281–296. https://doi.org/10.1016/s0035-1598(98)90197-0.

Jenkyns, H.C., 2010. Geochemistry of oceanic anoxic events. Geochemistry, Geophysics, Geosystems 11, Q03004. https://doi.org/10.1029/2009GC002788.

Jeremiah, J.M., 2001. A Lower Cretaceous nannofossil zonation for the North Sea Basin. Journal of Micropalaeontology 20, 45–80. https://doi.org/http:/dx.doi.org/10.1144/jm.20.1.45.

Jud, R., 1994. Biochronology and Systematics of Early Cretaceous Radiolaria of the Western Tethys. Mémoires de Géologie (Lausanne) 19, 147.

Kuhnt, W., Moullade, M., Masse, J.-P., Erlenkeuser, H., 1998. Carbon isotope stratigraphy of the lower Aptian historical stratotype at Cassis-La Bédoule (SE France). Géologie Méditérranéenne 25, 63–79. https://doi.org/10.3406/geolm.1998.1625.

Larson, R.L., Erba, E., 1999. Onset of the Mid-Cretaceous greenhouse in the Barremian-Aptian: Igneous events and the biological, sedimentary, and geochemical responses. Paleoceanography 14, 663–678. https://doi.org/10.1029/1999pa900040.

Li, Y.-X., Bralower, T.J., Montañez, I.P., Osleger, D.A., Arthur, M.A., Bice, D.M., Herbert, T.D., Erba, E., Premoli-Silva, I., 2008. Toward an orbital chronology for the early Aptian Oceanic Anoxic Event (OAE1a, ~120 Ma). Earth and Planetary Science Letters 271, 88–100. https://doi.org/10.1016/j.epsl.2008.03.055.

Linnert, C., Mutterlose, J., 2013. Biometry of Cenomanian–Turonian placoliths: a proxy for changes of fertility and surface-water temperature? Lethaia 46, 82–97. https://doi.org/10.1111/j.1502-3931.2012.00323.x.

Journal Pre-proof

López-Otálvaro, G.E., Suchéras-Marx, B., Giraud, F., Mattioli, E., Lécuyer, C., 2012. *Discorhabdus* as a key coccolith genus for paleoenvironmental reconstructions (Middle Jurassic, Lusitanian Basin): Biometry and taxonomic status. Marine Micropaleontology 94-95, 45–57. https://doi.org/https://do.org/10.1016/j.marmicro.2012.06.003.

Lübke, N., Mutterlose, J., 2016. The impact of OAE 1a on marine biota deciphered by size variations of coccoliths. Cretaceous Research 61, 169–179. https://doi.org/https://doi.og/10.1016/j.cretres.2016.01.006

Lübke, N., Mutterlose, J., Bottini, C., 2015. Size variations of coccoliths in Cretaceous oceans — A result of preservation, genetics and ecology? Marine Micropaleontology 117, 25–39. https://doi.org/10.1016/j.marmicro.2015.03.002.

Malinverno, A., Erba, E., Herbert, T.D., 2010. Orbital tuning as an inverse problem: Chronology of the early Aptian oceanic anoxic event 1a (Selli Level) in the Cismon APTICORE. Paleoceanography 25, 1–16. https://doi.org/10.1029/2009PA001769.

Malkoč, M., Mutterlose, J., Pauly, S., 2010. Timing of the Early Aptian $\delta^{13}C$ excursion in the Boreal Realm. Newsletters on Stratigraphy 43, 251–273. https://doi.org/10.1127/0078-0421/2010/0043-0251.

Martín-Chivelet, J., López-Gómez, J., Aguado, R., Arias, C., Arribas, J., Arribas, M.E., Aurell, M., Bádenas, B., Benito, M.I., Bover-Arnal, T., Casas-Sainz, A., Castro, J.M., Coruña, F., de Gea, G.A., Fornós, J.J., Fregenal-Martínez, M., García-Senz, J., Garófano, D., Gelabert, B., Giménez, J., González-Acebrón, L., Guimerà, J., Liesa, C.L., Mas, R., Meléndez, N., Molina, J.M., Muñoz, J.A., Navarrete, R., Nebot, M., Nieto, L.M., Omodeo-Salé, S., Pedrera, A., Peropadre, C., Quijada, I.E., Quijano, M.L., Reolid, M., Robador, A., Rodríguez-López, J.P., Rodríguez-Perea, A., Rosales, I., Ruiz-Ortiz, P.A., Sàbat, F., Salas, R., Soria, A.R., Suarez-Gonzalez, P., Vilas, L.,

Journal Pre-proof

2019. The Late Jurassic–Early Cretaceous Rifting, in: Quesada, C., Oliveira, J.T. (Eds.), The Geology of Iberia: A Geodynamic Approach. Regional Geology Reviews Volume 3, The Alpine Cycle. Springer, Heidelberg, pp. 169–249. https://doi.org/10.1007/978-3-030-11295-0_5.

Martinez, M., Aguado, R., Company, M., Sandoval, J., O'Dogherty, L., 2020. Integrated astrochronology of the Barremian Stage (Early Cretaceous) and its biostratigraphic subdivisions. Global and Planetary Change 195, 1–24. https://doi.org/10.1016/j.gloplacha.2020.103368.

Masse, J.P., Bellion, Y., Benkhelil, J., Ricou, L.E., Dercourt, J., Guiraud, R., 1993. Early Aptian (114–111 Ma), in: Dercourt, J., Ricou, L. E., Vrielynck, B. (Eds.), Atlas, Tethys, Palaeoenvironmental Maps. BEICIP-FRANLAB, Rueil-Malmaison.

Masse, J.-P., Machhour, L., 1998. La matière organique dans la série du stratotype historique de l'Aptien inférieur dans la région de Cassis-La Bédoule (SE France). Géologie Méditerranéenne 25, 55–62.

Moreno-Bedmar, J.A., Company, M., Bover-Arnal, T., Salas, R., Delanoy, G., Martínez, R., Grauges, A., 2009. Biostratigraphic characterization by means of ammonoids of the lower Aptian Oceanic Anoxic Event (OAE 1a) in the eastern Iberian Chain (Maestrat Basin, eastern Spain). Cretaceous Research 30, 864–872. https://doi.org/10.1016/j.cretres.2009.02.004.

Moreno-Bedmar, J.A., Company, M., Sandoval, J., Tavera, J.M., Bover-Arnal, T., Salas, R., Delanoy, G., Maurrasse, F.J.-M.R., Martínez, R., 2012. Lower Aptian ammonite and carbon isotope stratigraphy in the eastern Prebetic Domain (Betic Cordillera, southeastern Spain). Geologica Acta 10, 333–350.

Moullade, M., Kuhnt, W., Bergen, J.A., Masse, J.-P., Tronchetti, G., 1998a. Correlation of biostratigraphic and stable isotope events in the Aptian historical stratotype of La

Journal Pre-proof

Bédoule (southeast France). Comptes Rendus de l'Académie des Sciences de Paris, Sciences de la Terre et des Planètes 327, 693–698. https://doi.org/10.1016/s1251-8050(99)80027-5.

Moullade, M., Masse, J.-P., Tronchetti, G., Kuhnt, W., Ropolo, P., Bergen, J.A., Masure, E., Renard, M., 1998b. Le stratotype historique de l'Aptien inférieur (région de Cassis -La Bédoule, SE France): synthèse stratigraphique. Géologie Méditérranéenne 25, 289–298. https://doi.org/10.3406/geolm.1998.1641.

Mutterlose, J., 1987. Calcareous nannofossils and belemnites as warmwater indicators from the NW-German Middle Aptian. Geologisches Jahrbuch A96, 293–313.

Mutterlose, J., 1989. Temperature-controlled migration of calcareous nannofloras in the north-west European Aptian, in: Crux, J.A., Heck, S.E.V. (Eds.), Nannofossils and their Applications. British Micropalaeontological Society Publication Series. Ellis Horwood Ltd., Chichester, pp. 122–142.

Mutterlose, J., 1992a. Biostratigraphy and palaeobiogeography of Early Cretaceous calcareous nannofossils. Cretaceous Research 13, 167–189. https://doi.org/10.1016/0195-6671(92)90034-n.

Mutterlose, J., 1992b. Migration and evolution patterns of floras and faunas in marine Early Cretaceous sediments of NW Europe. Palaeogeography, Palaeoclimatology, Palaeoecology 94, 261–282. https://doi.org/10.1016/0031-0182(92)90123-m.

Mutterlose, J., 1996. Calcareous nannofossil paleoceanography of the Early Cretaceous of NW Europe. Mitteilungen der Geologisches-Paläontologisches Institut Universität Hamburg 77, 291–313.

Mutterlose, J., 1998. The Barremian-Aptian turnover of biota in northwestern Europe: evidence from belemnites. Palaeogeography, Palaeoclimatology, Palaeoecology 144, 161–173. https://doi.org/10.1016/s0031-0182(98)00081-9.

Journal Pre-proof

Mutterlose, J., Böckel, B., 1998. The Barremian - Aptian interval in NW Germany: a review. Cretaceous Research 19, 539–568. https://doi.org/10.1006/cres.1998.0119.

O'Dogherty, L., 1994. Biochronology and Paleontology of Mid-Cretaceous Radiolarians from Northern Apennines (Italy) and Betic Cordillera (Spain). Mémoires de Géologie (Lausanne) 21, 413.

Ogg, J.G., Ogg, G.M., Gradstein, F.M., 2016. A Concise Geologic Time Scale 2016, Elsevier, Amsterdam 234 pp.

Olierook, H.K.H., Jourdan, F., Merle, R.E., 2019. Age of the Barremian–Aptian boundary and onset of the Cretaceous Normal Superchron. Earth-Science Reviews 197, 1–22. https://doi.org/10.1016/j.earscirev.2019.102906.

Patruno, S., Triantaphyllou, M.V., Erba, E., Dimiza, M.D., Bottini, C., Kaminski, M.A., 2015. The Barremian and Aptian stepwise development of the 'Oceanic Anoxic Event 1a' (OAE 1a) crisis: Integrated benthic and planktic high-resolution palaeoecology along the Gorgo a Cerbara stratotype section (Umbria–Marche Basin, Italy). Palaeogeography, Palaeoclimatology, Palaeoecology 424, 147–182. https://doi.org/10.1016/j.palaeo.2015.01.031.

Perch-Nielsen, K., 1985. Mesozoic calcareous nannofossils, in: Bolli, H.M., Saunders, J.B., et al. (Eds.), Plankton Stratigraphy. Cambridge University Press, Cambridge, pp. 329–426.

Premoli Silva, I., Soldan, D.M., Petrizzo, M.R., 2018. Upper Hauterivian–upper Barremian planktonic foraminiferal assemblages from the Arroyo Gilico section (southern Spain). Journal of Foraminiferal Research 48, 314–355. https://doi.org/10.2113/gsjfr.48.4.314.

Quijano, M.L., Castro, J.M., Pancost, R.D., de Gea, G.A., Najarro, M., Aguado, R., Rosales, I., Martín-Chivelet, J., 2012. Organic geochemistry, stable isotopes, and

facies analysis of the Early Aptian OAE − New records from Spain (Western Tethys). Palaeogeography, Palaeoclimatology, Palaeoecology 365-366, 276–293. https://doi.org/10.1016/j.palaeo.2012.09.033.

Reboulet, S., Rawson, P.F., Moreno-Bedmar, J.A., Aguirre-Urreta, M.B., Barragan, R., Bogomolov, Y., Company, M., González-Arreola, C., Stoyanova, V.I., Lukeneder, A., Matrion, B., Mitta, V., Randrianaly, H., Vasicek, Z., Baraboschkin, E.J., Bert, D., Bersac, S., Bogdanova, T.N., Bulot, L., Latil, J.L., Mikhailova, I.A., Ropolo, P., Szives, O., 2011. Report on the 4th International Meeting of the IUGS Lower Cretaceous Ammonite Working Group, the "Kilian Group" (Dijon, France, 30th August 2010). Cretaceous Research 32, 786–793 https://doi.org/10.1016/j.cretres.2011.05.007.

Reboulet, S., Szives, O., Aguirre-Urreta, M.B., Barragán, R., Company, M., Frau, C., Kakabadze, M., Klein, J., Moreno-Bedmar, J.A., Lukeneder, A., Pictet, A., Ploch, I., Raisossadat, S.N., Vašíček, Z., Baraboshkin, E., Mitta, V.V., 2018. Report on the 6th International Meeting of the IUGS Lower Cretaceous Ammonite Working Group, the Kilian Group (Vienna, Austria, 20th August 2017). Cretaceous Research 91, 100–110. https://doi.org/10.1016/j.cretres.2018.05.008.

Roth, P.H., 1978. Cretaceous nannoplankton biostratigraphy and oceanography of the northwestern Atlantic ocean, in: Benson, W.E., Sheridan, R.E., et al. (Eds.), Initial Reports of the Deep Sea Drilling Project 44. U. S. Government Printing Office, Washington, pp. 731–759.

Roth, P.H., 1983. Jurassic and Lower Cretaceous calcareous nannofossils in the western north Atlantic (Site 534): biostratigraphy, preservation, and some observations on biogeography and paleoceanography, in: Sheridan, R.E., Gradstein, F.M., et al.

Journal Pre-proof

(Eds.), Initial Reports of the Deep Sea Drilling Project 76. U. S. Government Printing Office, Washington, pp. 587–621.

Roth, P.H., 1994. Distribution of coccoliths in oceanic sediments. In: Winter, A., Siesser, W.G. (Eds.), Coccolithophores. Cambridge University Press, Cambridge, pp. 199–218.

Roth, P.H., Thierstein, H.R., 1972. Calcareous nannoplankton: Leg 14 of the Deep Sea Drilling Project, in: Hayes, D.E., Pimm, A.C., et al. (Eds.), Initial Reports of the Deep Sea Drilling Project 14. U. S. Government Printing Office, Washington, pp. 421–485.

Rutledge, D.C., Bown, P.R., 1996. New names for old: taxonomic clarification of some Early Cretaceous nannofossil marker-species. Journal of Nannoplankton Research 18, 53–59.

Sanchez-Hernandez, Y., Maurrasse, F.J.-M.R., 2016. The influence of regional factors in the expression of oceanic anoxic event 1a (OAE1a) in the semi-restricted Organyà Basin, south-central Pyrenees, Spain. Palaeogeography, Palaeoclimatology, Palaeoecology 441, 582–598. https://doi.org/10.1016/j.palaeo.2015.06.031.

Sissingh, W., 1977. Biostratigraphy of Cretaceous calcareous nannoplankton. Geologie en Mijnbouw 56, 37–65.

Sprovieri, M., Coccioni, R., Lirer, F., Pelosi, N., Lozar, F., 2006. Orbital tuning of a lower Cretaceous composite record (Maiolica Formation, central Italy). Paleoceanography 21, PA4212, doi:4210.1029/2005PA001224. https://doi.org/10.1029/2005PA001224.

Stampfli, G.M., Kozur, H.W., 2006. Europe from the Variscan to the Alpine cycles, in: Gee, D.G., Stephenson, R.A. (Eds.), European Lithosphere Dynamics, 32. The Geological Society, London, pp. 57–81.

Journal Pre-proof

Stein, M., Föllmi, K.B., Westermann, S., Godet, A., Adatte, T., Matera, V., Fleitmann, D., Berner, Z., 2011. Progressive palaeoenvironmental change during the Late Barremian–Early Aptian as prelude to Oceanic Anoxic Event 1a: Evidence from the Gorgo a Cerbara section (Umbria-Marche basin, central Italy). Palaeogeography, Palaeoclimatology, Palaeoecology 302, 396–406. https://doi.org/10.1016/j.palaeo.2011.01.025.

Street, C., Bown, P.R., 2000. Palaeobiogeography of Early Cretaceous (Berriasian-Barremian) calcareous nannoplankton. Marine Micropaleontology 39, 265–291. https://doi.org/10.1016/s0377-8398(00)00024-4.

Thierstein, H.R., 1971. Tentative Lower Cretaceous calcareous nannoplankton zonation. Eclogae Geologicae Helvetiae 64, 459–488.

Thierstein, H.R., 1973. Lower Cretaceous calcareous nannoplankton biostratigraphy. Abhandlungen der Geologischen Bundes-Anstalt 29, 1–52.

Thierstein, H.R., 1976. Mesozoic calcareous nannoplankton biostratigraphy of marine sediments. Marine Micropaleontology 1, 325–362. https://doi.org/10.1016/0377-8398(76)90015-3.

Tremolada, F., Erba, E., Bralower, T.J., 2006. Late Barremian to early Aptian calcareous nannofossil paleoceanography and paleoecology from the Ocean Drilling Program Hole 641C (Galicia Margin). Cretaceous Research 27, 887–897. https://doi.org/10.1016/j.cretres.2006.04.007.

Triantaphyllou, M., Dimiza, M., Krasakopoulou, E., Malinverno, E., Lianou,V., Souvermezoglou, E., 2010. Seasonal variation in *Emiliania huxleyi* coccolith morphology and calcification in the Aegean Sea (Eastern Mediterranean). Geobios 43, 99–110.

Journal Pre-proof

Vera, J.A., 2001. Evolution of the Southern Iberian Continental Margin, in: Ziegler, P.A., Cavazza, W., Robertson, A.H.F., Crasquin-Soleau, S. (Eds.), Peri-Tethyan Rift/Wrench Basins and Passive Margins, 186. Mémoires du Muséum National d'Histoire Naturelle Paris, pp. 109–143.

Vera, J.A., 2004. Cordillera Bética y Baleares. In: Vera, J.A. (Ed.), Geología de España.Sociedad Geológica de España e Instituto Geológico y Minero de España, Madrid, pp. 345–464.

Wissler, L., Weissert, H.J., Masse, J.-P., Bulot, L., 2002. Chemostratigraphic correlation of Barremian and lower Aptian ammonite zones and magnetic reversals. International Journal of Earth Sciences (Geologische Runschau) 91, 272–279. https://doi.org/10.1007/s005310100210.

Wulff, L., Mutterlose, J., Bornemann, A., 2020. Size variations and abundance patterns of calcareous nannofossils in mid Barremian black shales of the Boreal Realm (Lower Saxony Basin). Marine Micropaleontology 156, 1–14. https://doi.org/10.1016/j.marmicro.2020.101853.

Yilmaz, I.O., Altiner, D., Tekin, U.K., Ocakoglu, F., 2012. The first record of the "Mid-Barremian" Oceanic Anoxic Event and the Late Hauterivian platform drowning of the Bilecik platform, Sakarya Zone, western Turkey. Cretaceous Research 38, 16–39. https://doi.org/10.1016/j.cretres.2012.04.010.

Young, J.R., Bergen, J.A., Bown, P.R., Burnett, J.A., Fiorentino, A., Jordan, R.W., Kleijne, A., Van Niel, B., Romein, A.J.T., Von Salis, K., 1997. Guidelines for coccolith and calcareous nannofossil terminology. Palaeontology 40, 875–912.

Zhang, Y., Ogg, J.G., Minguez, D.A., Hounslow, M.W., Olaussen, S., 2021. Magnetostratigraphy of U-Pb–dated boreholes in Svalbard, Norway, implies that

magnetochron M0r (a proposed Barremian-Aptian boundary marker) begins at 121.2 ± 0.4 Ma. Geology 49. https://doi.org/10.1130/G48591.1.

Ziegler, P.A., 1990. Geological Atlas of Western and Central Europe. Shell Internationale Petroleum Mij. B.V. and Geological Society, London, 239 p.

Figure 1. Geologic sketch of the central and eastern sectors of the Betic Cordillera, showing the present-day location of the sections included in this study. A: X.Cp_2 section; B: X.V_1 section; C: X.Kv and X.Kv_2 sections; D: X.Ag_6 section; E: RA03 section; F: X.CT and X.HA sections; G: X.Z section; H: X.F and X.F1 sections; I: X.CO_2 section.

Figure 2. Paleogeographic map of the Western Tethys–Atlantic connection for the late Barremian (~123 Ma) with indication of the paleolatitude (modified from Ziegler, 1990 and Barrier et al., 2018). Location of several areas and sections referenced throughout the text. Sb: Subbetic Basin. 398: DSDP Site 398 (Bralower et al., 1994); 603: DSDP Site 603 (Covington and Wise, 1987); 641: ODP Site 641 (Bralower et al., 1994); Cg: UK North Sea Central Graben (Well 22/26a-2); Mf: Moray-Firth area (Well 21/2-6); Nj: North Jens-1 Well; Sp: Speeton cliffs (see Jeremiah, 2001). Gp: Gargano Promontory (Cobianchi et al., 1997); Ls: Lower Saxony Basin (Malkoč et al., 2010).

Figure 3. Lithologic sketches of sections X.V_1, X.Kv, X.Kv_2 and RA03, with indication of formations, stage, ammonite/calcareous nannofossil biostratigraphy, thickness, position and number (in parentheses) of samples studied and main calcareous nannofossil bioevents recorded. Marker species names are in bold typeface.

Journal Pre-proof

Figure 4. Lithologic sketches of sections X.Ag_6, X.CT, X.Z, X.HA, X.F1, X.F, X.CO_2 and X.Cp_2, with indication of formations, stage, ammonite/calcareous nannofossil biostratigraphy, thickness, position and number of samples studied and main calcareous nannofossil bioevents recorded. Marker species names are in bold typeface.

Figure 5. Cross-plot of width (W) vs. length (L) for 120 upper Barremian *Lithraphidites* spp. specimens. A–D: Cross-plots of width *vs.* length for the different taxa and sketches of the side and top views of each one (upper right), with indication of measured parameters. E, F: Frequency histograms of the width (E) and length (F) of the complete data set. The distribution curves in E result from a mixture analysis applied to the whole data set using the widths of all measured *Lithraphidites* spp. specimens. G: Frequency histogram showing the distribution curves resulting from a mixture analysis applied to the length of all measured specimens having a width greater than 5 µm. H: Table showing the descriptive statistical parameters (proportion, mean, and standard deviation) of the mixture analyses performed on the width and length of the measured specimens. Dashed vertical lines on the cross-plot are the widths suggested to separate *Lithraphidites carniolensis* from the new species *L. aichmoides* (3 µm) and *L. aichmoides* from the *L. magnus*/*L. pugio* plexus (5 µm). Circles with cross on the graph indicate the calculated mean values for each species/group of taxa. W was measured in the area with the maximum expansion of the blades of *Lithaphidites* spp.

Figure 6. Cross-plot of length/width (L/W) ratio *vs.* length (L) for 69 *Lithraphidites* specimens of the *L. pugio*/*L. magnus* plexus. Note as all specimens assigned to *L. magnus* have L >24 µm and L/W ratio >3.5, being located within the upper right quadrant of the graph.

Figure 7. A. Parameters measured in 140 specimens of the *Hayesites irregularis* group. B) Cross-plot of L vs. W. Shaded dots indicate initially assumed *H. irregularis* E. Regression lines considering all specimens (solid) and the separated populations of *H. irregularis* s.str. and *H. irregularis* E (dashed). C) Frequency histogram showing the distribution curves resulting from a mixture analysis applied to the L/W ratio of all measured specimens. The small table shows the descriptive statistical parameters (proportion, mean, and standard deviation) resulting from the mixture analysis. Two populations are revealed based on the L/W ratio. The forms with L/W > 1.12 were assigned to *H. irregularis* E. See text for details.

Figure 8. X.- Cross-plot of coccolith length (L) vs. width (W) for 120 specimens of *Flabellites oblongus* s.l., referred to ammonite zones (different symbols for data points), with frequency histograms of the complete data set. The distribution curves on the histograms result from applying mixture analyses. Dashed-line curves (A) result from the discrimination of two populations within the whole data set. Solid continuum line curves (B) result from the discrimination of only one population in the complete data set. Y.- Table showing the descriptive statistical parameters resulting from the mixture analyses, where the two options (A and B) are considered. Mout = *Holcodiscus caillaudianus* ASz + *Moutoniceras moutonianum* AZ; Vand =*Toxancyloceras vandenheckii* AZ; Sart =*Gerhardtia sartousiana* ASz; Prov =*Gerhardtia provincialis* ASz; Fera =*Hemihoplites feraudianus* ASz; Gira=*Imerites giraudi* AZ; Sara=*Martelites sarasini* AZ; Ogla=*Deshayesites oglanlensis* AZ; Forb=*Deshayesites forbesi* AZ. Numbers in parentheses represent the specimens measured in each interval. Note the

nearly continuous distribution of the coccolith size, where two populations can not be clearly differentiated and the close AIC values for cases A and B.

Figure 9. Geochronostratigraphic sketch showing a compilation of the main biostratigraphic events recorded in this study. Geochronology and ammonite stratigraphy after Martinez et al. (2020). Positions of the MBE (Mid-Barremian Episode) TE (Taxy Episode) and C-isotope Intra-Sarasini Negative Excursion (ISNE) are based on data from Martinez et al. (2020). Calcareous nannofossil subzones are those proposed here. The stratigraphic ranges of all new species described in present study and the newly described calcareous nannofossil subzones are calibrated to ammonite zones and to geochronology. Ranges with black lines correspond to marker species. Intervals of the species ranges with very rare/spotty record are marked with dashed line. Numbers in parentheses refer to the numerical ages (in Ma) of the bioevents associated to zonal markers using the chronology of Martinez et al. (2020). The wc>nc horizon indicates the stratigraphic position where the wide-canal nannoconids outnumber the narrow canal nannoconids (wc>nc Event).

Figure 10. Correlation of the uppermost Barremian–lowermost Aptian interval of the sections of Barranco de Cavila ($X.Kv_2$), Angles, Casis-La Bédoule and Gorgo a Cerbara using ammonite and C-isotope data. Light green shaded band correspond to the ISNE associated to the Taxy Episode. Light blue shaded band correspond to the OAE 1a. Lines of correlation: dashed lines based on ammonite biostratigraphy, dotted-dashed lines are based on calcareous nannofossils, and dotted line is based on C-isotope curves. Data for $X.Kv_2$ section after Martinez et al. (2020) and this paper; data for Cassis-La Bédoule after Kuhnt et al (1998) and Moullade et al. (1998a); data for Angles after

Delanoy (1995), Wissler et al. (2002) and Godet et al. (2006); data for Gorgo a Cerbara after Stein et al. (2011, 2012) and Frau et al. (2018). In Angles section, the boundary between *Martelites sarasini* and *Deshayesites oglanlensis* AZs marked with a star is after Godet et al. (2006), the boundary marked with two stars (bed 197b) is after Delanoy (1995), and reinterpreted here following Reboulet et al. (2011).

Figure 11. Proposed morpho-evolutionary sketch for the genus *Lithraphidites* across the late Barremian–early late Aptian. Chronostratigraphic scale following Martinez et al. (2020). Calcareous nannofossil zones/subzones follow Bralower et al. (1995) and modifications proposed in this work. Tethyan ammonite zones after Reboulet et al. (2018). NW Europe ammonite zones follow Mutterlose (1992b), Casey et al. (1998), Mutterlose and Böckel (1998), Malkoč et al. (2010), and Bottini and Mutterlose (2012). Stratigraphic range of *Lithraphidites bouchtonii* and *Lithraphidites moray-firthensis* after Jeremiah (2001) and Bottini and Mutterlose (2012). Sea-level curves (dashed line = long-term; continuous line = short-term) after Hardenbol et al. (1998). MBE = Mid-Barremian Episode, TE = Taxy Episode, ISNE = C-isotope Intra-Sarasini Negative Excursion. Duration of the MBE, TE and ISNE after Martinez et al. (2020). Duration of the OAE 1a after Li et al. (2008), Malinverno et al. (2010) and Giraud et al. (2018).

Figure 12. Cross-polarized light micrographs of several specimens of some of the new species described here. Holotypes/paratypes are indicated. Species name and section - sample of provenance are shown for each one.

Figure 13. Cross-polarized light micrographs of several specimens of some of the new species described here. Holotypes/paratypes are indicated. Species name and section - sample of provenance are shown for each one.

Figure 14. Cross-polarized light micrographs of several specimens of some of the new/emended species described here. Holotypes/paratypes are indicated. Species name and section - sample of provenance are shown for each one.

Figure 15. Cross-polarized light micrographs of several specimens of the *Hayesites irregularis* group, with differentiation of the two morphotypes described in the text and *Nannoconus* sp. cf. *N. truittii*. Species name and section - sample of provenance are shown for each one.

Highlights

- Seven new upper Barremian nannofossil species are described.
- Tethyan upper Barremian calcareous nannofossil biostratigraphy is improved.
- The latest Barremian $\delta^{13}C$ excursion should be considered as a potential marker for the base of the Aptian.
- Calcareous nannofossil morpho-evolutionary trends were controlled by paleogeography.

Journal Pre-proof

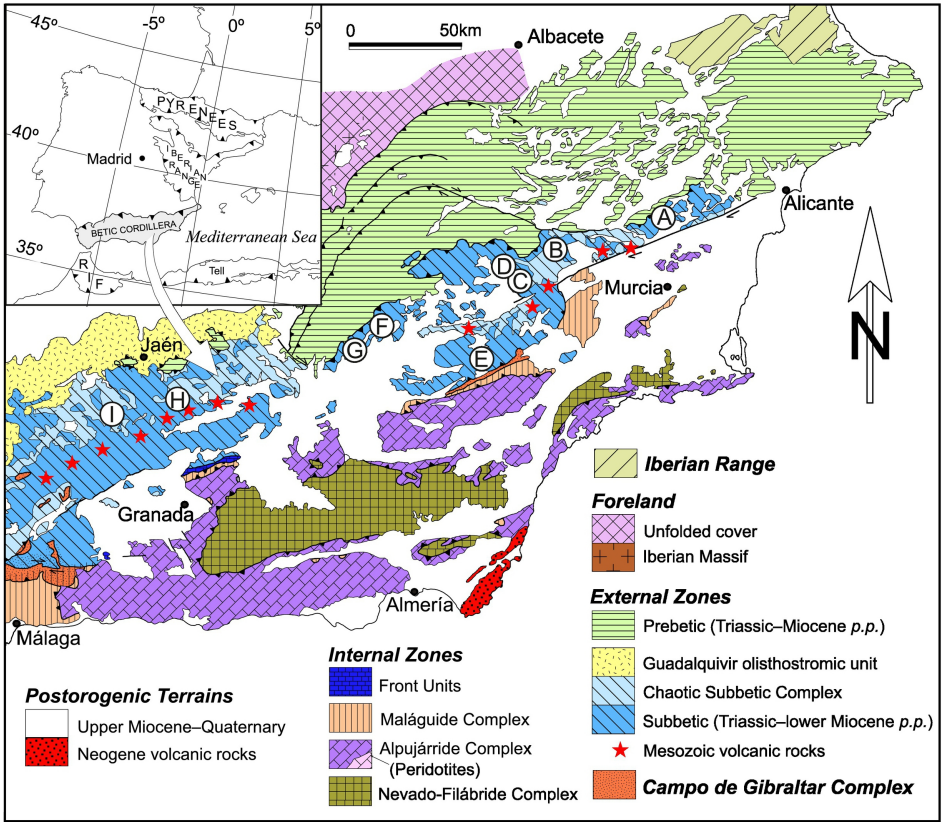
45º
-5º
0º
5º
40º
35º
PYRENEES
IBERIAN RANGE
Madrid
BETIC CORDILLERA
Mediterranean Sea
Tell
R
F
0
50km
Albacete
Alicante
Murcia
Jaén
Granada
Almeria
Málaga
A
B
C
D
E
F
G
H
I
N
Iberian Range
Foreland
Unfolded cover
Iberian Massif
External Zones
Prebetic (Triassic–Miocene p.p.)
Guadalquivir olisthostromic unit
Chaotic Subbetic Complex
Subbetic (Triassic–lower Miocene p.p.)
Mesozoic volcanic rocks
Campo de Gibraltar Complex
Internal Zones
Front Units
Maláguide Complex
Alpujárride Complex
(Peridotites)
Nevado-Filábride Complex
Postorogenic Terrains
Upper Miocene–Quaternary
Neogene volcanic rocks

Figure 1

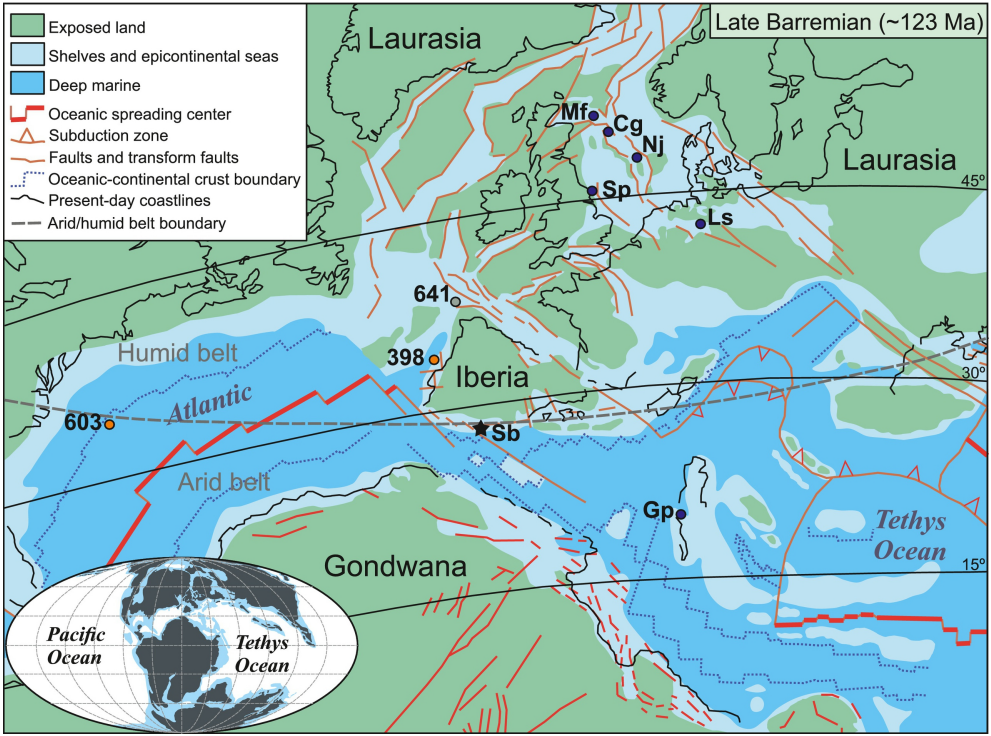
Exposed land
Shelves and epicontinental seas
Deep marine
Oceanic spreading center
Subduction zone
Faults and transform faults
Oceanic-continental crust boundary
Present-day coastlines
Arid/humid belt boundary
Late Barremian (~123 Ma)
Laurasia
Laurasia
Mf
Cg
Nj
Sp
Ls
45°
641
398
Iberia
Humid belt
Atlantic
603
Sb
30°
30
Arid belt
Gp
Tethys Ocean
Gondwana
15°
Pacific Ocean
Tethys Ocean

Figure 2

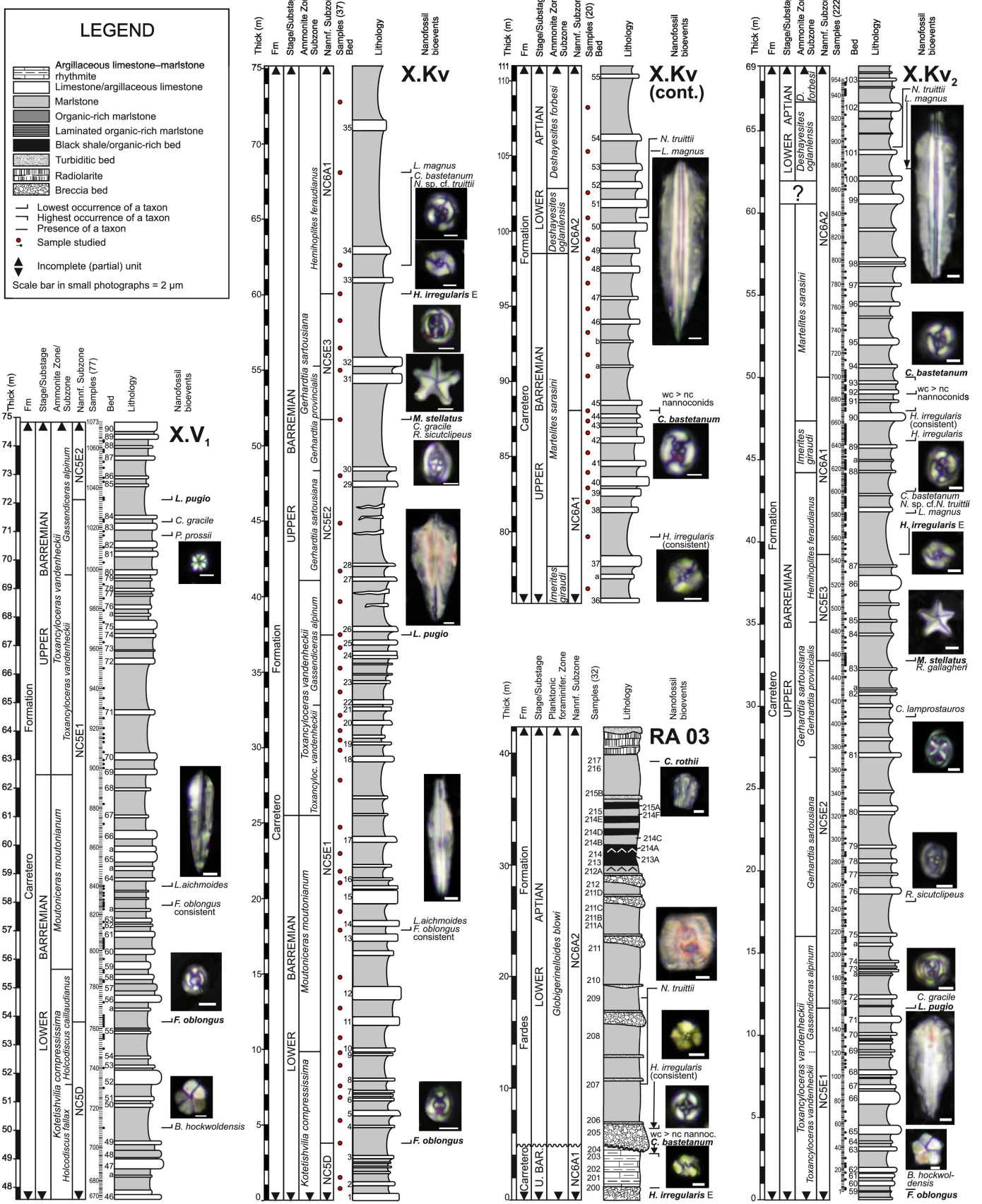
LEGEND
Argillaceous limestone–marlstone rhythmite
Limestone/argillaceous limestone
Marlstone
Organic-rich marlstone
Laminated organic-rich marlstone
Black shale/organic-rich bed
Turbiditic bed
Radiolarite
Breccia bed
Lowest occurrence of a taxon
Highest occurrence of a taxon
Presence of a taxon
Sample studied
Incomplete (partial) unit
Scale bar in small photographs = 2 µm
X.V1
X.Kv
X.Kv (cont.)
RA 03
X.Kv2
Thick (m)
Fm
Stage/Substage
Ammonite Zone/ Subzone
Nannf. Subzone
Samples
Bed
Lithology
Nanofossil bioevents
Carretero Formation
Fardes Formation
UPPER BARREMIAN
LOWER BARREMIAN
LOWER APTIAN
Toxancyloceras vandenheckii
Gassendiceras alpinum
Moutoniceras moutonianum
Kotetishvilia compressissima
Holcodiscus callaudianus
Globigerinelloides blowi
Gerhardtia sartousiana
Gerhardtia provincialis
Hemiholpites feraudianus
Martelites sarasini
Imerites giraudi
Deshayesites forbesi
Deshayesites oglanlensis
L. pugio
C. gracile
P. prossii
L.aichmoides
F. oblongus consistent
F. oblongus
B. hockwoldensis
L. magnus
C. bastetanum
N. sp. cf. truittii
H. irregularis E
M. stellatus
C. gracile
R. sicutclipeus
wc > nc nannoconids
N. truittii
H. irregularis (consistent)
wc > nc nannoc.
C. rothii
R. gallagheri
C. lamprostauros
B. hockwol-densis

Figure 3

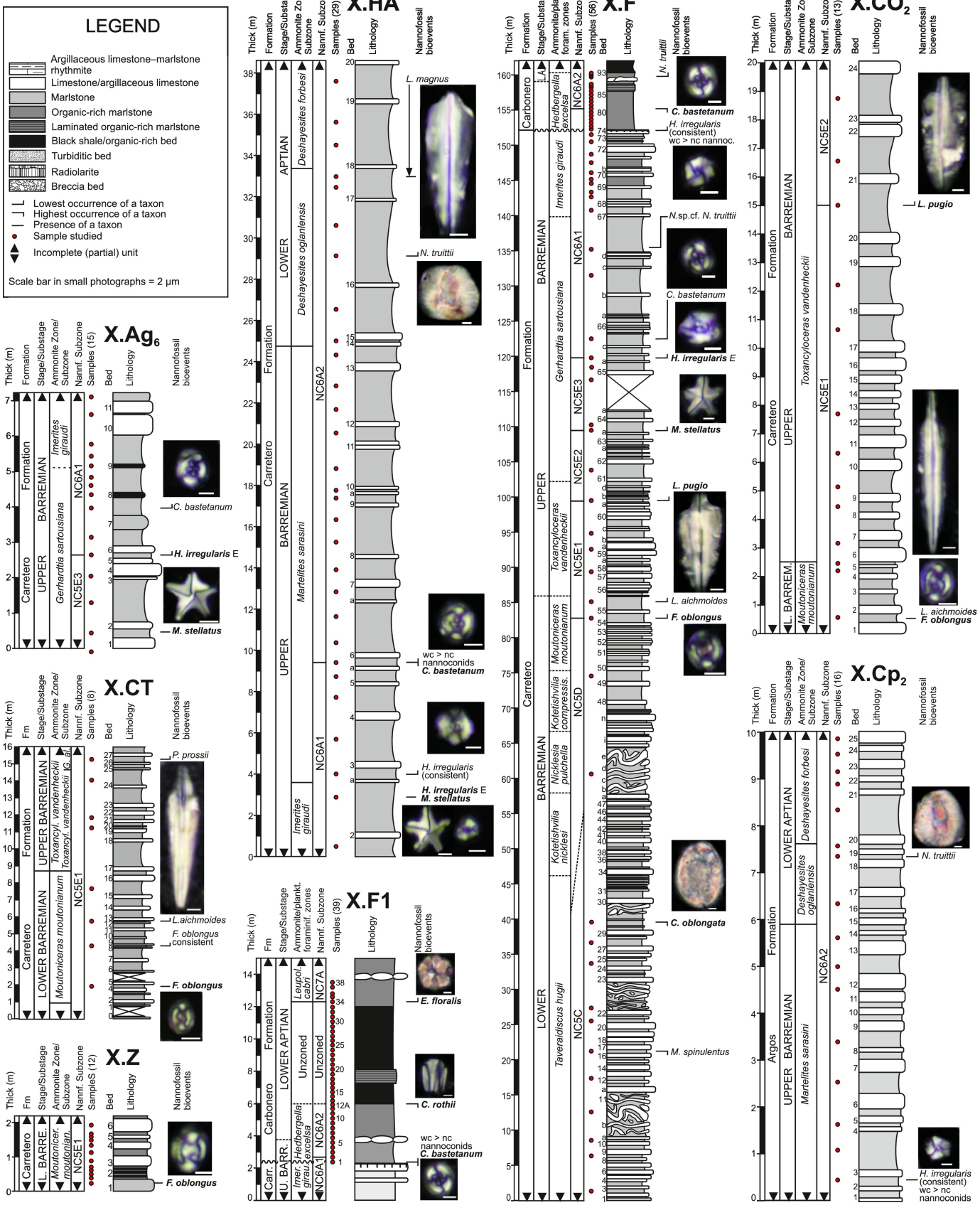
LEGEND
Argillaceous limestone–marlstone rhythmite
Limestone/argillaceous limestone
Marlstone
Organic-rich marlstone
Laminated organic-rich marlstone
Black shale/organic-rich bed
Turbiditic bed
Radiolarite
Breccia bed
Lowest occurrence of a taxon
Highest occurrence of a taxon
Presence of a taxon
Sample studied
Incomplete (partial) unit
Scale bar in small photographs = 2 µm
X.Ag6
X.CT
X.Z
X.HA
X.F1
X.F
X.CO2
X.Cp2
Thick (m)
Formation
Stage/Substage
Ammonite Zone/ Subzone
Nannof. Subzone
Samples
Bed
Lithology
Nannofossil bioevents
Carretero
UPPER BARREMIAN
Gerhardtia sartousiana
Imerites giraudi
NC6A1
NC5E3
C. bastetanum
H. irregularis E
M. stellatus
LOWER BARREMIAN
Moutoniceras moutonianum
Toxancyl. vandenheckii
NC5E1
P. prossii
L. aichmoides
F. oblongus consistent
F. oblongus
L. BARRE.
Moutonicer. moutonian.
Carr.
U. BARR.
Carbonero
LOWER APTIAN
Hedbergella excelsa
Unzoned
NC6A2
NC7A
E. floralis
C. rothii
wc > nc nannoconids
C. bastetanum
Argos
Taveraldiscus hugii
Kotetishvilia nicklesi
Nicklesia pulchella
Kotetishvilia compressis.
Moutoniceras moutonianum
Toxancyloceras vandenheckii
Gerhardtia sartousiana
Imerites giraudi
Hedbergella excelsa
NC5C
NC5D
NC5E2
NC6A1
NC5E3
L. magnus
N. truittii
wc > nc nannoconids
C. bastetanum
H. irregularis (consistent)
H. irregularis E
M. stellatus
Martelites sarasini
Deshayesites oglanlensis
Deshayesites forbesi
NC6A2
N. truittii
H. irregularis (consistent) wc > nc nannoc.
N.sp.cf. N. truittii
C. bastetanum
H. irregularis E
M. stellatus
L. pugio
L. aichmoides
F. oblongus
C. oblongata
M. spinulentus
Toxancyloceras vandenheckii
Moutoniceras moutonianum
L. BARREM.
NC5E1
NC5E2
L. pugio
L. aichmoides
F. oblongus
Martelites sarasini
Deshayesites oglanlensis
Deshayesites forbesi
N. truittii
H. irregularis (consistent) wc > nc nannoconids

Figure 4

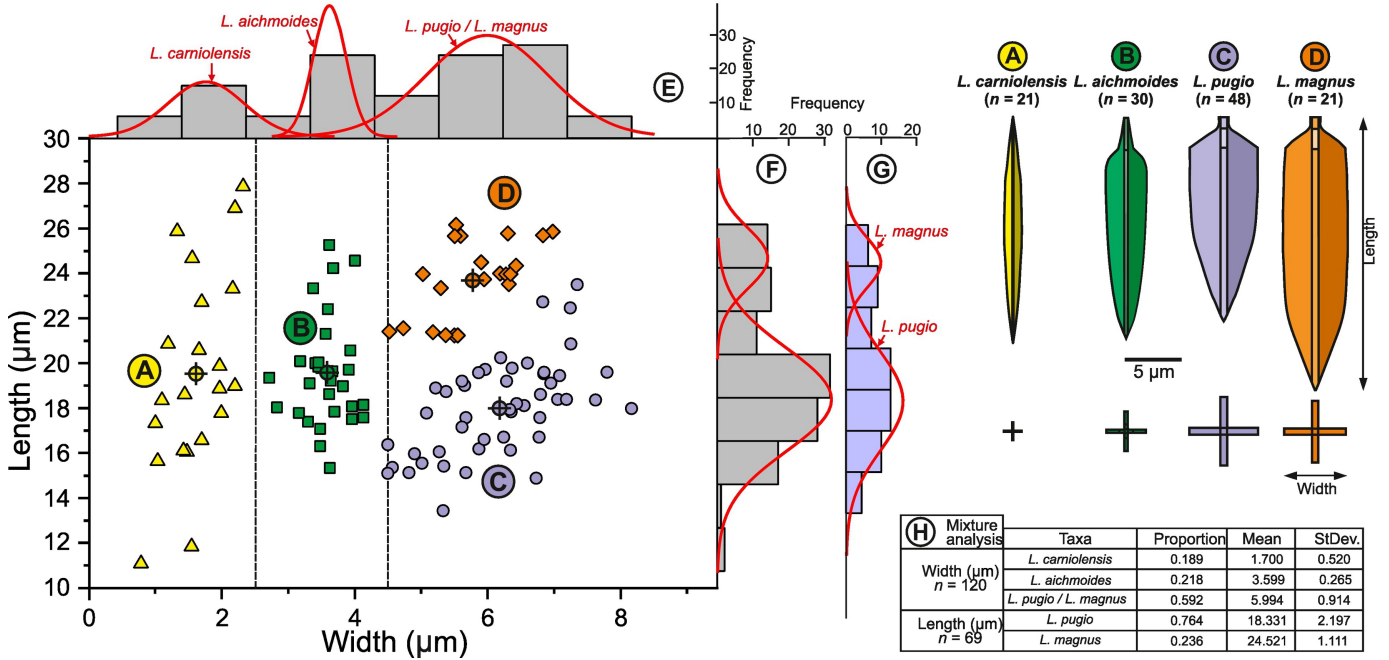

H Mixture analysis	Taxa	Proportion	Mean	StDev.
Width (µm) n = 120	*L. carniolensis*	0.189	1.700	0.520
	L. aichmoides	0.218	3.599	0.265
	L. pugio / L. magnus	0.592	5.994	0.914
Length (µm) n = 69	*L. pugio*	0.764	18.331	2.197
	L. magnus	0.236	24.521	1.111

Figure 5

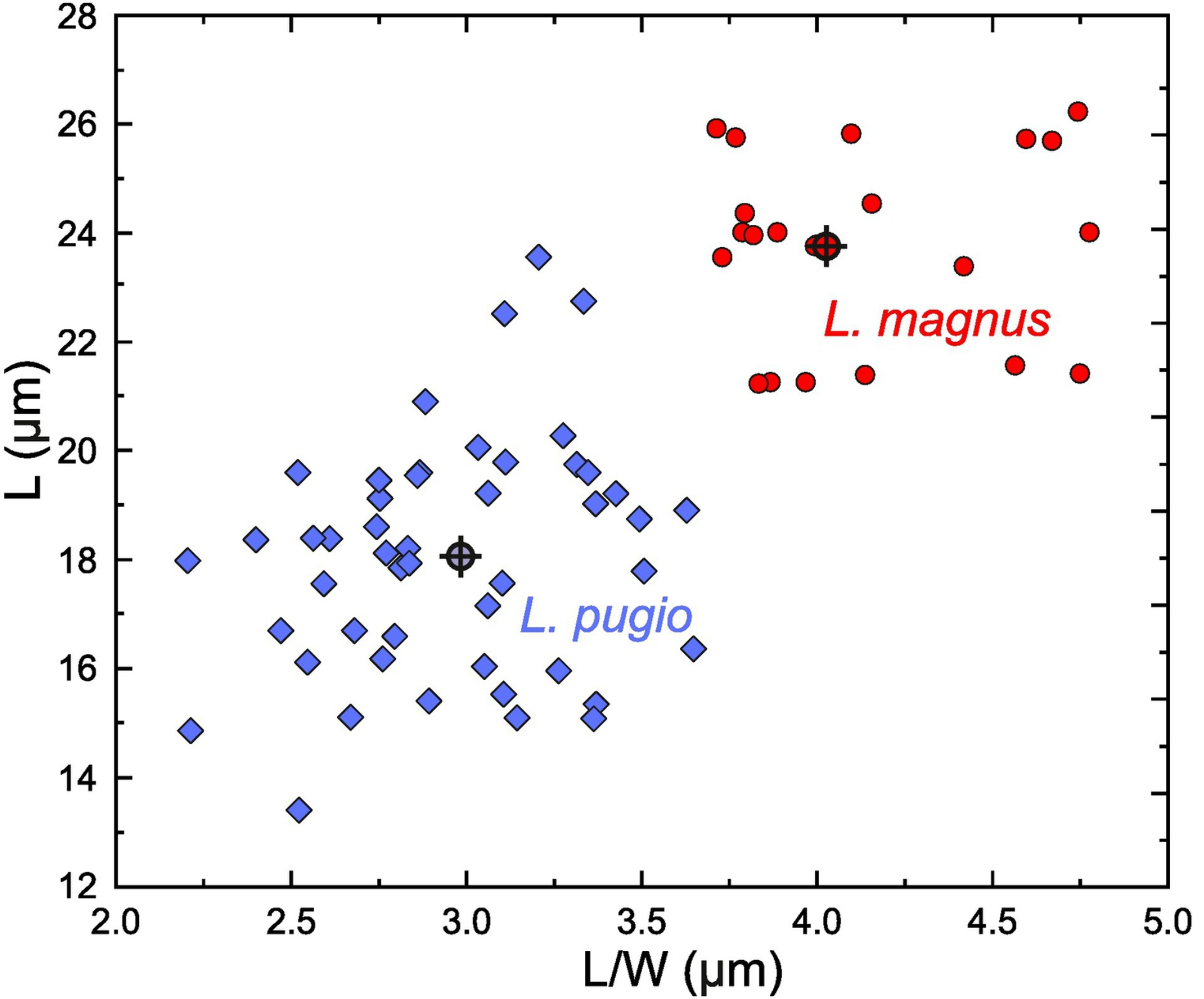
28
26
24
22
20
18
16
14
12
L (µm)
2.0
2.5
3.0
3.5
4.0
4.5
5.0
L/W (µm)
L. magnus
L. pugio

Figure 6

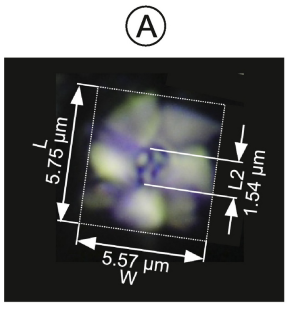
A
L
5.75 µm
L2
1.54 µm
5.57 µm
W

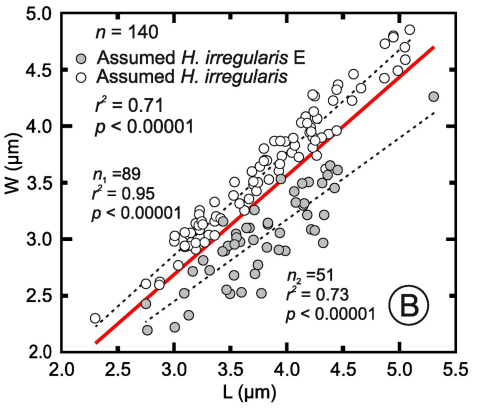
n = 140
Assumed H. irregularis E
Assumed H. irregularis
r² = 0.71
p < 0.00001
n1 =89
r² = 0.95
p < 0.00001
n2 =51
r² = 0.73
p < 0.00001
B
W (µm)
L (µm)
5.0
4.5
4.0
3.5
3.0
2.5
2.0
2.0
2.5
3.0
3.5
4.0
4.5
5.0
5.5

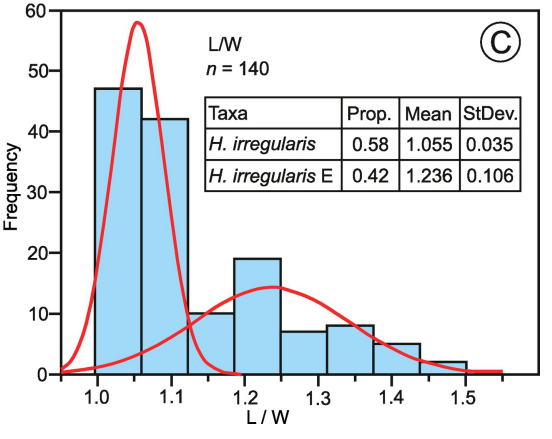
C
L/W
n = 140
Taxa | Prop. | Mean | StDev.
H. irregularis | 0.58 | 1.055 | 0.035
H. irregularis E | 0.42 | 1.236 | 0.106
Frequency
L / W
60
50
40
30
20
10
0
1.0
1.1
1.2
1.3
1.4
1.5

Figure 7

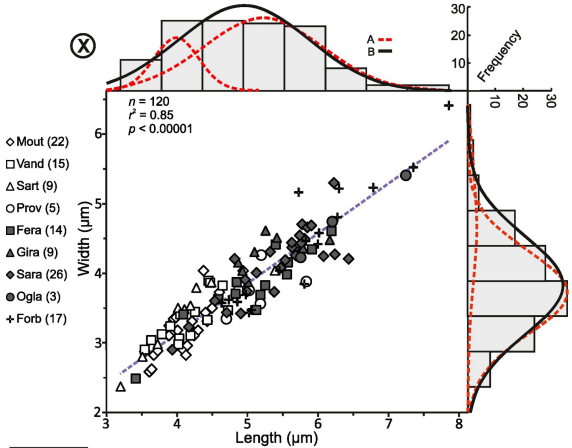

Y Mixture analysis	Case	AIC	Population	Proportion	Mean	StDev.
Length (µm) n = 120	A	95.1	1	0.217	3.994	0.315
			2	0.783	5.223	0.827
	B	99.3	1	1	4.956	0.902
Width (µm) n = 120	A	37.6	1	0.891	3.721	0.600
			2	0.109	4.695	0.836
	B	38.3	1	1	3.827	0.699

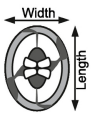

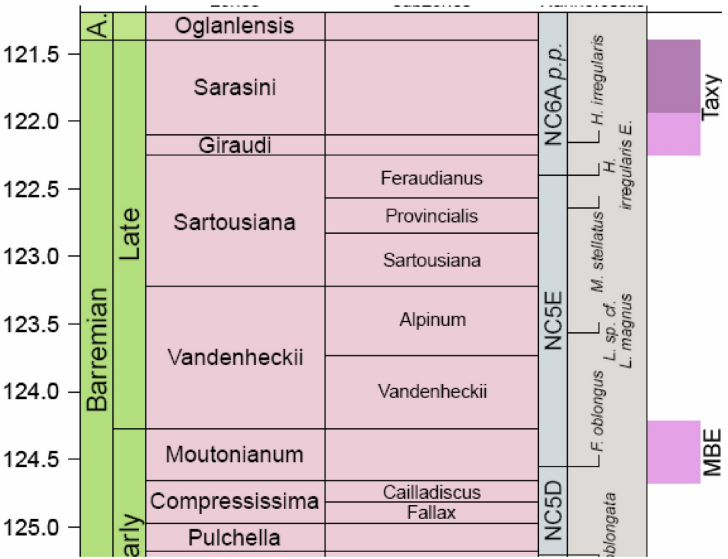

Figure 8

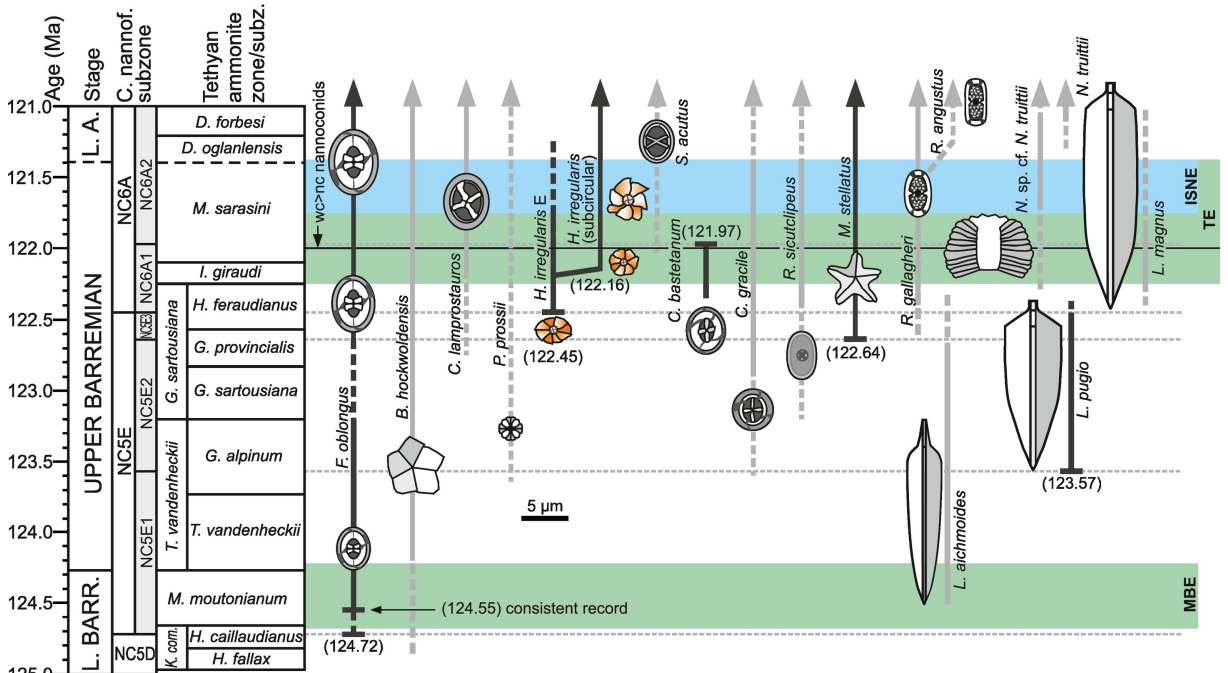
Age (Ma)
Stage
C. nannof. subzone
Tethyan ammonite zone/subz.
121.0
121.5
122.0
122.5
123.0
123.5
124.0
124.5
125.0
L. A.
UPPER BARREMIAN
L. BARR.
NC6A
NC5E
NC5D
NC6A2
NC6A1
NC5E2
NC5E1
D. forbesi
D. oglanlensis
M. sarasini
I. giraudi
H. feraudianus
G. provincialis
G. sartousiana
G. alpinum
T. vandenheckii
M. moutonianum
H. caillaudianus
H. fallax
G. sartousiana
T. vandenheckii
K. com.
wc>nc nannoconids
F. oblongus
B. hockwoldensis
C. lamprostauros
P. prossii
H. irregularis E
H. irregularis (subcircular)
(122.16)
(122.45)
S. acutus
C. bastetanum
(121.97)
C. gracile
R. siculiclipeus
M. stellatus
(122.64)
R. gallagheri
R. angustus
N. sp. cf. N. truittii
N. truittii
L. magnus
L. pugio
(123.57)
L. aichmoides
5 µm
(124.55) consistent record
(124.72)
ISNE
TE
MBE

Figure 9

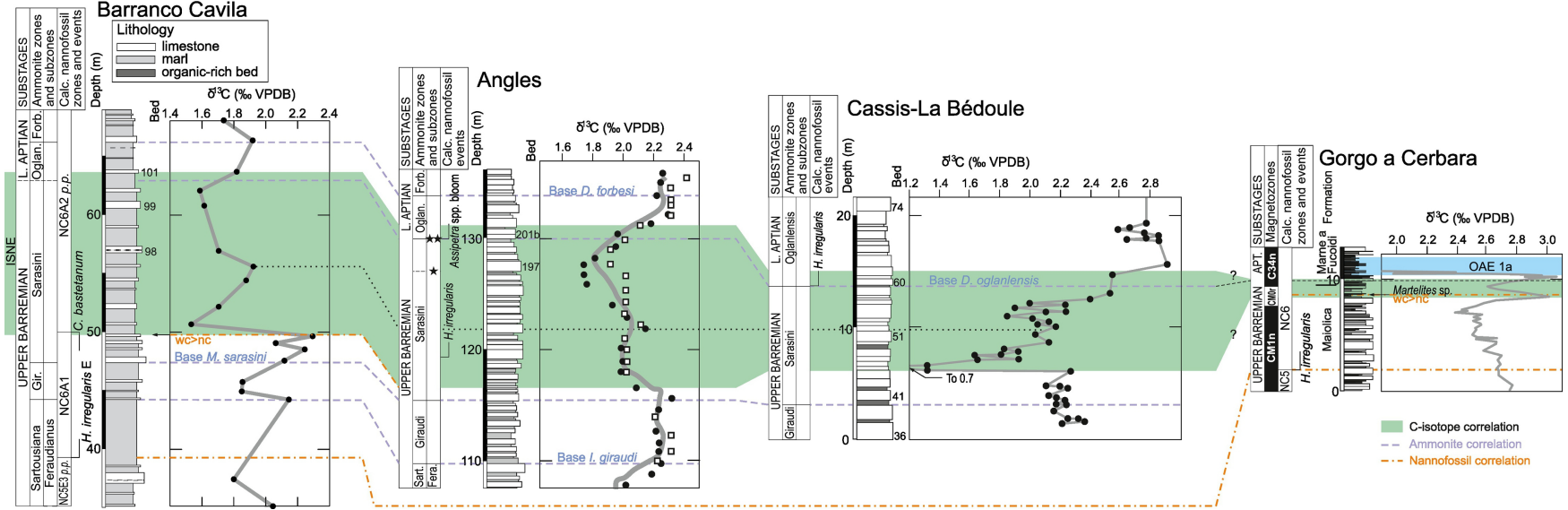
Barranco Cavila
Lithology
limestone
marl
organic-rich bed
Depth (m)
δ13C (‰ VPDB)
Bed
wc>nc
Base M. sarasini
Angles
Base D. forbesi
Base I. giraudi
Cassis-La Bédoule
Base D. oglanlensis
To 0.7
Gorgo a Cerbara
OAE 1a
Marne a Fucoidi
Maiolica
Martelites sp.
wc>nc
C-isotope correlation
Ammonite correlation
Nannofossil correlation

Figure 10

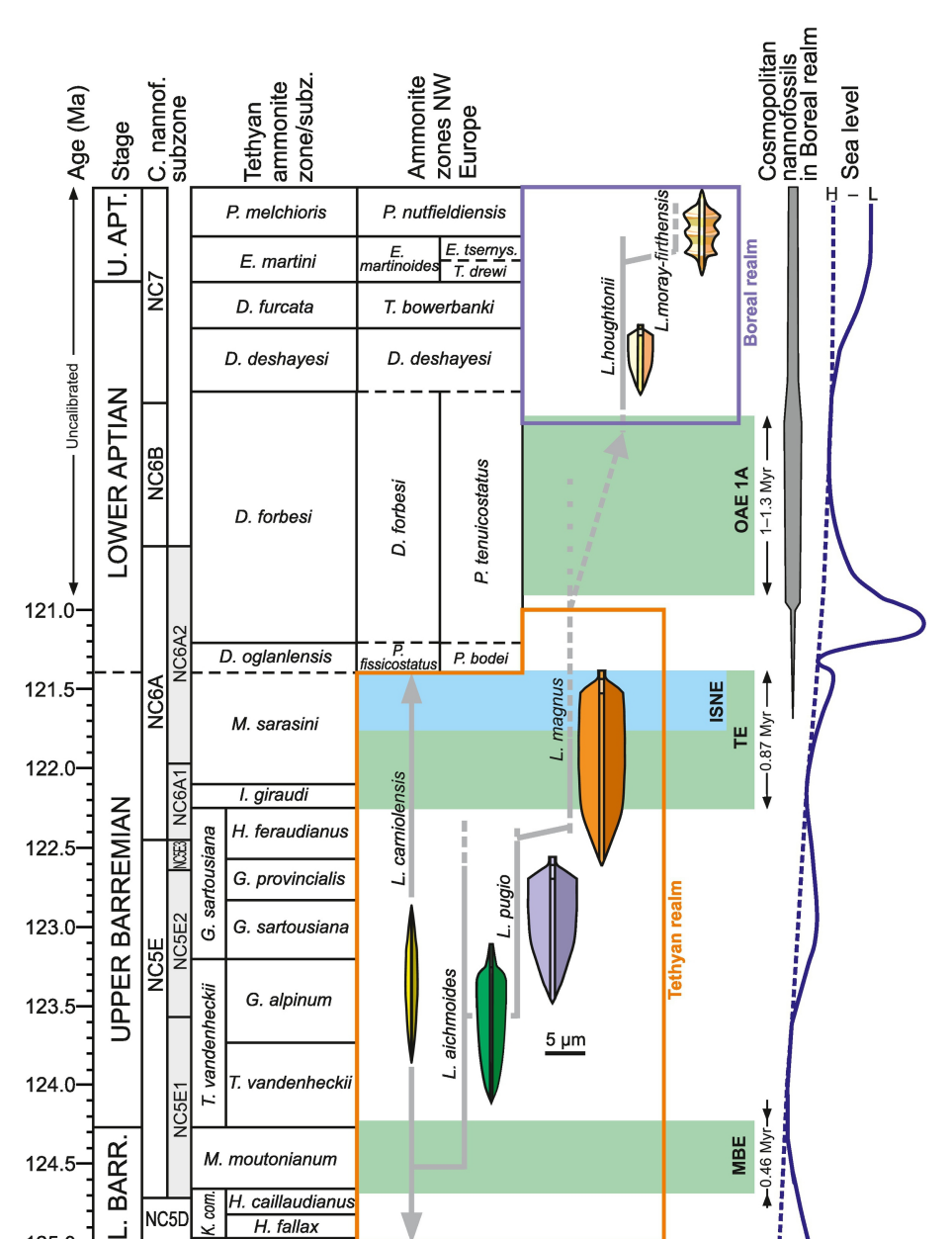
Age (Ma)
Stage
C. nannof. subzone
Tethyan ammonite zone/subz.
Ammonite zones NW Europe
Cosmopolitan nannofossils in Boreal realm
Sea level
Uncalibrated
121.0
121.5
122.0
122.5
123.0
123.5
124.0
124.5
125.0
L. BARR.
UPPER BARREMIAN
LOWER APTIAN
U. APT.
NC5D
NC5E1
NC5E2
NC5E3
NC6A1
NC6A2
NC6A
NC6B
NC7
K. com.
T. vandenheckii
G. sartousiana
H. caillaudianus
H. fallax
M. moutonianum
T. vandenheckii
G. alpinum
G. sartousiana
G. provincialis
H. feraudianus
I. giraudi
M. sarasini
D. oglanlensis
D. forbesi
D. deshayesi
D. furcata
E. martini
P. melchioris
P. fissicostatus
P. bodei
P. tenuicostatus
D. forbesi
D. deshayesi
T. bowerbanki
E. martinoides
E. tsernys.
T. drewi
P. nutfieldiensis
L. carniolensis
L. aichmoides
L. pugio
L. magnus
L. houghtonii
L. moray-firthensis
5 µm
Tethyan realm
Boreal realm
MBE
TE
ISNE
OAE 1A
0.46 Myr
0.87 Myr
1–1.3 Myr

Figure 11

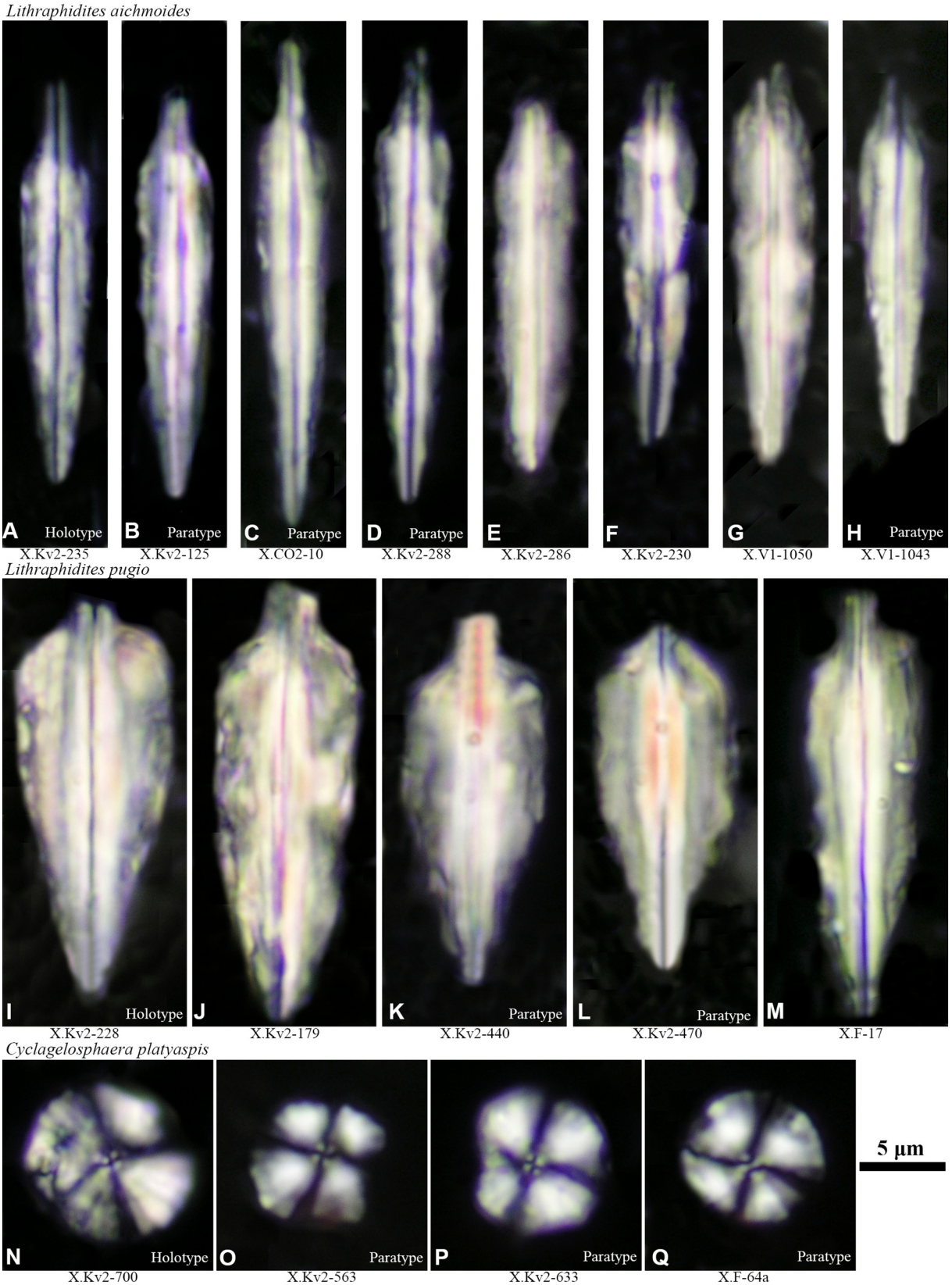
Lithraphidites aichmoides
A Holotype
X.Kv2-235
B Paratype
X.Kv2-125
C Paratype
X.CO2-10
D Paratype
X.Kv2-288
E
X.Kv2-286
F
X.Kv2-230
G
X.V1-1050
H Paratype
X.V1-1043
Lithraphidites pugio
I Holotype
X.Kv2-228
J
X.Kv2-179
K Paratype
X.Kv2-440
L Paratype
X.Kv2-470
M
X.F-17
Cyclagelosphaera platyaspis
N Holotype
X.Kv2-700
O Paratype
X.Kv2-563
P Paratype
X.Kv2-633
Q Paratype
X.F-64a
5 µm

Figure 12

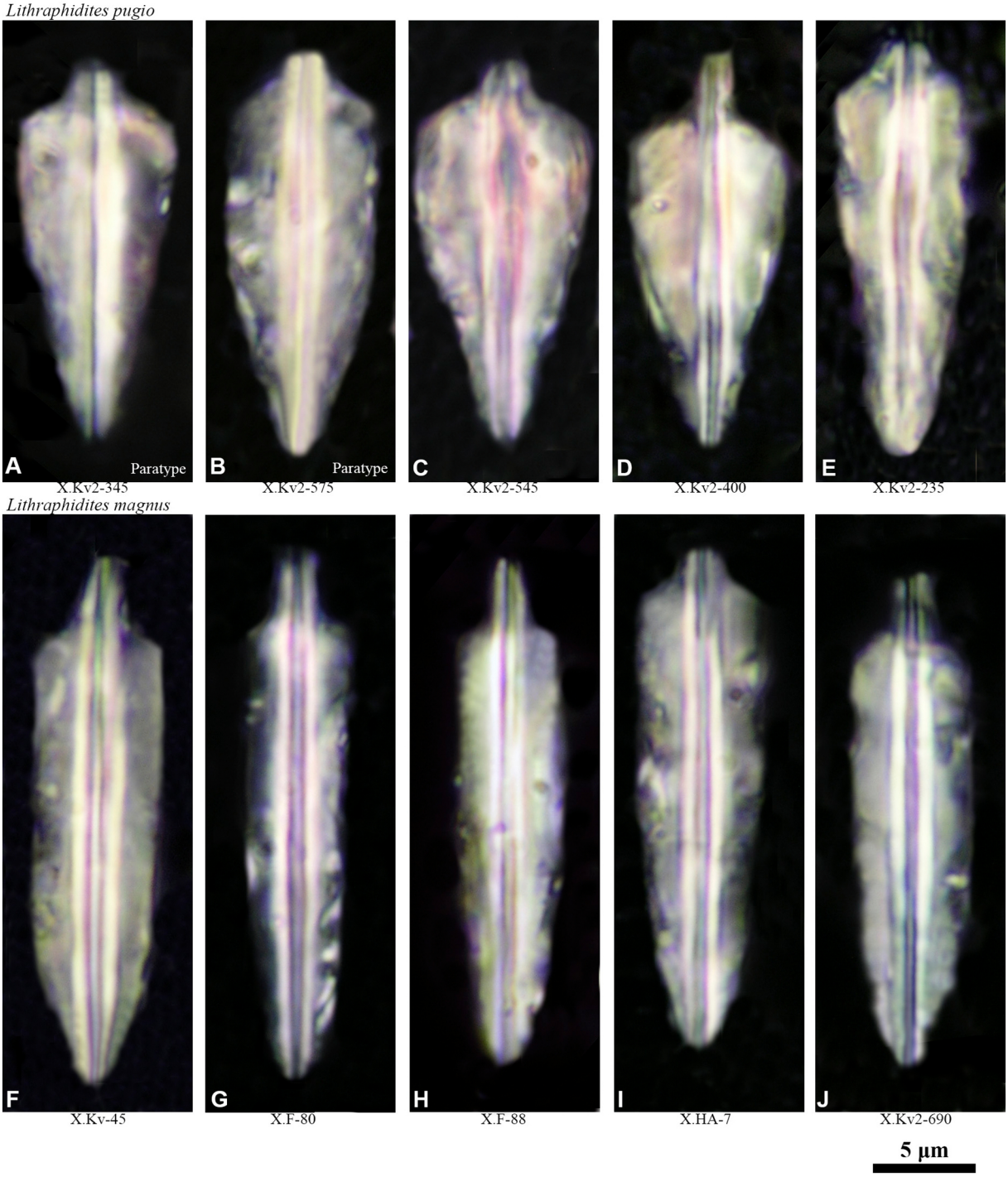
Lithraphidites pugio
A
Paratype
X.Kv2-345
B
Paratype
X.Kv2-575
C
X.Kv2-545
D
X.Kv2-400
E
X.Kv2-235
Lithraphidites magnus
F
X.Kv-45
G
X.F-80
H
X.F-88
I
X.HA-7
J
X.Kv2-690
5 µm

Figure 13

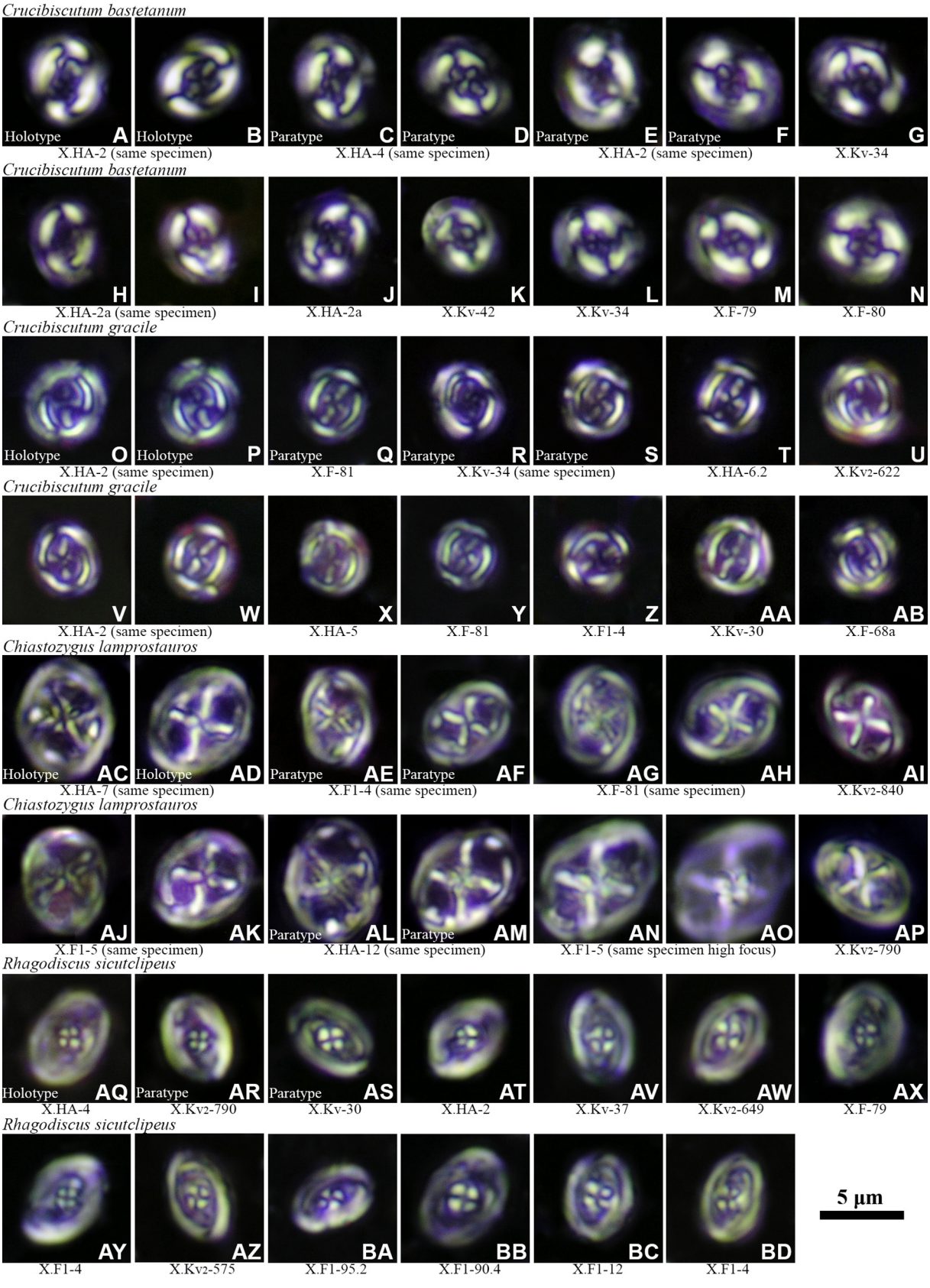
Crucibiscutum bastetanum
Holotype A
X.HA-2 (same specimen)
Holotype B
X.HA-4 (same specimen)
Paratype C
Paratype D
X.HA-2 (same specimen)
Paratype E
Paratype F
X.Kv-34
G
Crucibiscutum bastetanum
H
X.HA-2a (same specimen)
I
X.HA-2a
J
X.Kv-42
K
X.Kv-34
L
X.F-79
M
X.F-80
N
Crucibiscutum gracile
Holotype O
X.HA-2 (same specimen)
Holotype P
X.F-81
Paratype Q
X.Kv-34 (same specimen)
Paratype R
X.HA-6.2
Paratype S
X.Kv2-622
T
U
Crucibiscutum gracile
V
X.HA-2 (same specimen)
W
X.HA-5
X
X.F-81
Y
X.F1-4
Z
X.Kv-30
AA
X.F-68a
AB
Chiastozygus lamprostauros
Holotype AC
X.HA-7 (same specimen)
Holotype AD
X.F1-4 (same specimen)
Paratype AE
Paratype AF
X.F-81 (same specimen)
AG
X.Kv2-840
AH
AI
Chiastozygus lamprostauros
AJ
X.F1-5 (same specimen)
AK
X.HA-12 (same specimen)
Paratype AL
Paratype AM
X.F1-5 (same specimen high focus)
AN
X.Kv2-790
AO
AP
Rhagodiscus sicutclipeus
Holotype AQ
X.HA-4
Paratype AR
X.Kv2-790
Paratype AS
X.Kv-30
AT
X.HA-2
AV
X.Kv-37
AW
X.Kv2-649
AX
X.F-79
Rhagodiscus sicutclipeus
AY
X.F1-4
AZ
X.Kv2-575
BA
X.F1-95.2
BB
X.F1-90.4
BC
X.F1-12
BD
X.F1-4
5 µm

Figure 14

Hayesites irregularis E (early elongated form)

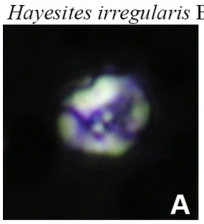

X.Kv2-576

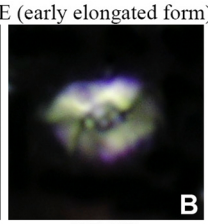

X.F-66D

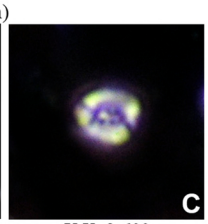

X.Kv2-600

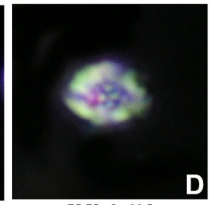

X.Kv2-605

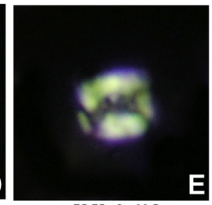

X.Kv2-605

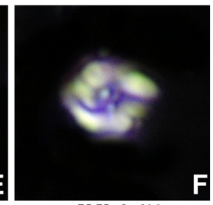

X.Kv2-611

Hayesites irregularis E (early elongated form)

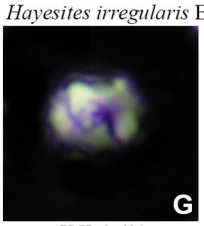

X.Kv2-621

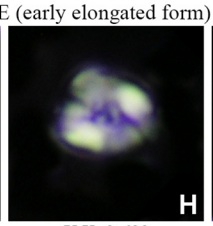

X.Kv2-622

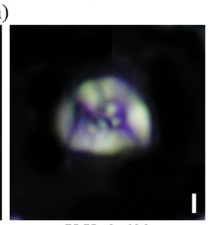

X.Kv2-633

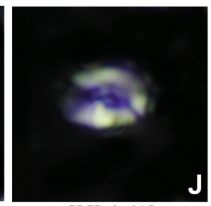

X.Kv2-645

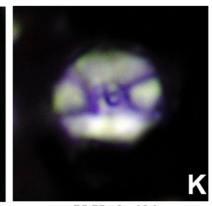

X.Kv2-680

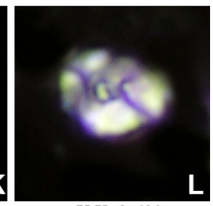

X.Kv2-690

Hayesites irregularis E (early elongated form)

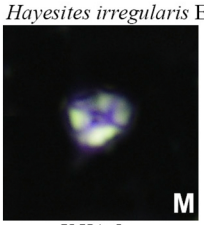

X.HA-5a

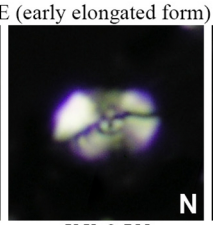

X.Kv2-755

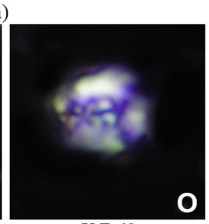

X.F-68a

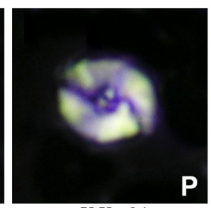

X.Kv-34

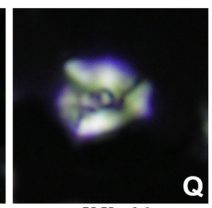

X.Kv-36

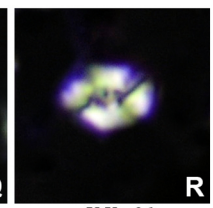

X.Kv-36

Hayesites irregularis (late subcircular form)

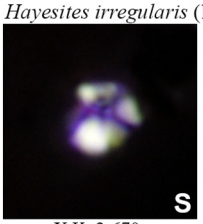

X.Kv2-670

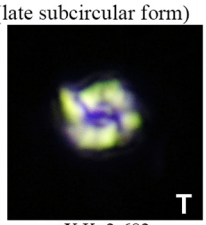

X.Kv2-682

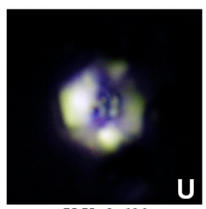

X.Kv2-690

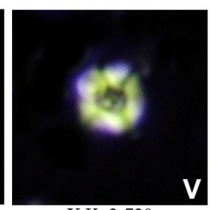

X.Kv2-720

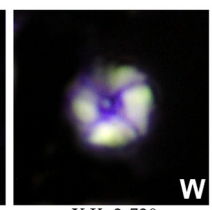

X.Kv2-720

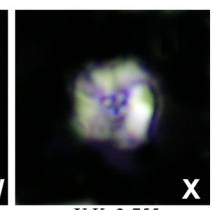

X.Kv2-755

Hayesites irregularis (late subcircular form)

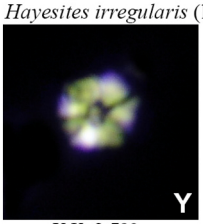

X.Kv2-790

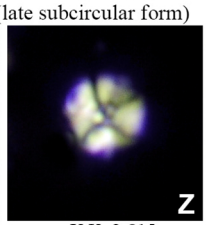

X.Kv2-815

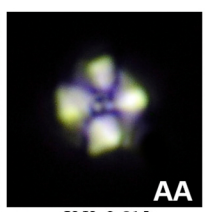

X.Kv2-815

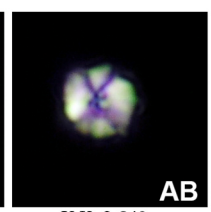

X.Kv2-840

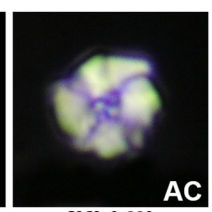

X.Kv2-882

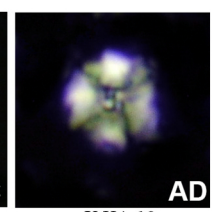

X.HA-10

Hayesites irregularis (late subcircular form)

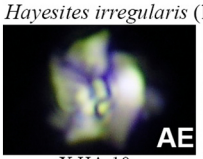

X.HA-10

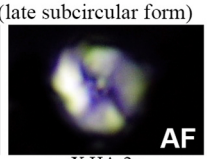

X.HA-2a

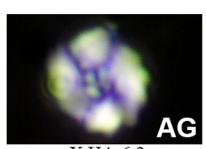

X.HA-6.2

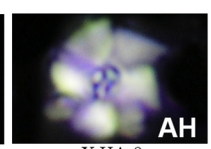

X.HA-9

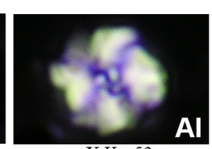

X.Kv-53

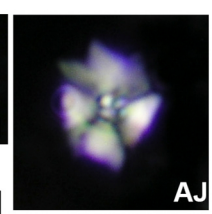

X.F-93

Nannoconus sp. cf. *N. truittii*

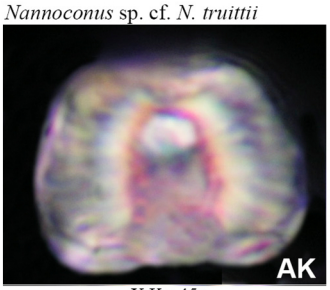

X.Kv-45a

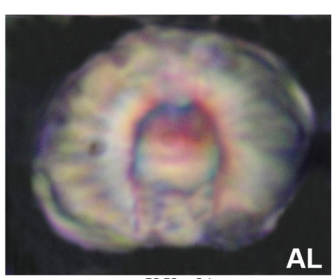

X.Kv-54

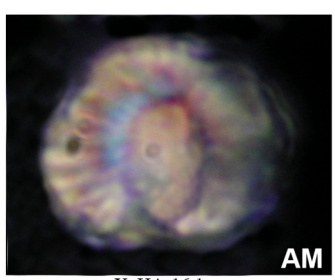

X..HA-16.1

5 µm

Figure 15